Available online at www.sciencedirect.com
ScienceDirect
Icarus 190 (2007) 179–202
ICARUS
www.elsevier.com/locate/icarus

Iapetus' geophysics: Rotation rate, shape, and equatorial ridge

J.C. Castillo-Rogez [a,*], D.L. Matson [a], C. Sotin [a,b], T.V. Johnson [a], J.I. Lunine [c], P.C. Thomas [d]

[a] *Jet Propulsion Laboratory, California Institute of Technology, M/S 230-260, 4800 Oak Grove Drive, Pasadena, CA 91109, USA*
[b] *UMR – CNRS 6112 Laboratoire de planétologie et géodynamique de Nantes, 2, rue de la Houssinière, 44322 Nantes Cedex 3, France*
[c] *Lunar and Planetary Laboratory, 1629 E. University Blvd., Tucson, AZ 85721-0092, USA*
[d] *Department of Astronomy, Cornell University, 422 Space Sciences Building, Ithaca, NY 14853, USA*

Received 23 July 2006; revised 30 January 2007

Available online 28 March 2007

Abstract

Iapetus has preserved evidence that constrains the modeling of its geophysical history from the time of its accretion until now. The evidence is (a) its present 79.33-day rotation or spin rate, (b) its shape that corresponds to the equilibrium figure for a hydrostatic body rotating with a period of ∼16 h, and (c) its high, equatorial ridge, which is unique in the Solar System. This paper reports the results of an investigation into the coupling between Iapetus' thermal and orbital evolution for a wide range of conditions including the spatial distributions with time of composition, porosity, short-lived radioactive isotopes (SLRI), and temperature. The thermal model uses conductive heat transfer with temperature-dependent conductivity. Only models with a thick lithosphere and an interior viscosity in the range of about the water ice melting point can explain the observed shape. Short-lived radioactive isotopes provide the heat needed to decrease porosity in Iapetus' early history. This increases thermal conductivity and allows the development of the strong lithosphere that is required to preserve the 16-h rotational shape and the high vertical relief of the topography. Long-lived radioactive isotopes and SLRI raise internal temperatures high enough that significant tidal dissipation can start, and despin Iapetus to synchronous rotation. This occurred several hundred million years after Iapetus formed. The models also constrain the time when Iapetus formed because the successful models are critically dependent upon having just the right amount of heat added by SLRI decay in this early period. The amount of heat available from short-lived radioactivity is not a free parameter but is fixed by the time when Iapetus accreted, by the canonical concentration of ^{26}Al, and, to a lesser extent, by the concentration of ^{60}Fe. The needed amount of heat is available only if Iapetus accreted between 2.5 and 5.0 Myr after the formation of the calcium aluminum inclusions as found in meteorites. Models with these features allow us to explain Iapetus' present synchronous rotation, its fossil 16-h shape, and the context within which the equatorial ridge arose.

Keywords: Iapetus; Interiors; Geophysics; Satellites, shapes; Satellites, dynamics

1. Introduction

Iapetus is the most distant, regular satellite of Saturn. Peale (1986) noted that Iapetus' synchronous rotation period of 79.33 days is unexpected considering its large distance from Saturn (i.e., an orbit with a 3.51×10^6 km semi-major axis, or ∼60 saturnian radii, R_S). Recent measurements by Cassini of Iapetus' low density and disequilibrium shape have made this satellite's dynamical state even more anomalous.

We have revisited this anomaly using coupled thermal- and dynamical-evolutionary modeling. We used recently determined parameters for material properties and Iapetus' characteristics (see Tables 1 and 2). The most recent Iapetus data were obtained by the *Cassini* mission during the close flyby of Iapetus on December 31, 2005.

Section 2 of this paper is a discussion of the three outstanding geophysical properties of Iapetus that constrain its origin: its rotation state, its shape, and the presence of the equatorial ridge.

Section 3 describes the model and assumptions. We discuss the main constraints, which are imposed by initial composition and structure. The effects of possible compositions are tested by

* Corresponding author. Fax: +1 818 393 4217.
E-mail address: julie.c.castillo@jpl.nasa.gov (J.C. Castillo-Rogez).

0019-1035/$ – see front matter
doi:10.1016/j.icarus.2007.02.018

Table 1
Iapetus' physical properties

Parameter (unit)	Value	Reference
Mean radius (km)	735.6 ± 3.0 km	Thomas et al. (2007)
Biaxial ellipsoid radii (km)	$747.4 \pm 3.1 \times 712.4 \pm 2.0$	Thomas et al. (2007)
Min–max radii (km)	35.0 ± 3.7	Thomas et al. (2007)
GM (km^3/s^2)	120.5117 ± 0.0173	Jacobson et al. (2006)
Density (kg/m^3)	1083 ± 13	Thomas et al. (2007)

Note. Gravitational constant: $G = 6.672(59 \pm 84) \times 10^{-11}$ kg^{-1} m^3 s^{-2}.

Table 2
Iapetus' dynamical properties

Parameter (unit)	Value	Reference
Semi-major axis (km)	3.5613×10^6	Yoder (1995)
Semi-major axis (R_{Saturn})	59.09	Yoder (1995)
Orbital period (days)	79.330183	Yoder (1995)
Orbital rate (rad/s)	9.1670093×10^{-7}	Yoder (1995)
Rotation period (days)	Synchronous	Yoder (1995)
Rotation rate (rad/s)	9.1670093×10^{-7}	Yoder (1995)
Eccentricity	0.0283	Yoder (1995)
Inclination (degrees)	7.52	Yoder (1995)

Note. R_{Saturn}: Saturn's radius = 60,268 km (equatorial radius).

varying the starting conditions: differing amounts of radionuclides and a range of volatile content. In terms of structure, we find that porosity is very important and its evolution must be included in the models.

Section 4 discusses the results of the modeling. We find self-consistent models, which lead to Iapetus' present-day rotation and shape. All of these successful models require formation of Iapetus early and inclusion of significant amounts of short-lived radioactive isotopes (SLRI). The main difficulty in modeling Iapetus is a shortage of heat. Without including SLRI we were not able to find realistic models that despin and still have the correct shape. Since the amount of SLRI heat needed for a particular model maps directly to formation time, one obtains the time of accretion for that model.

The models do not explicitly tell us about the formation of the equatorial ridge. However, through the prediction of decreasing surface area on Iapetus during despinning to synchronous rotation they provide a possible rationale as to why the ridge formed. Tracking surface area versus time provides some times when the ridge may have been formed.

Section 5 is a discussion of the broader implications of the models. Included are modeling techniques, convection, ridge formation, comparison with other satellites, the origin of Iapetus, and absolute chronometry and its implications.

Iapetus is a very intriguing object. Due to its circumstances, it did not have enough heat to evolve as far as other satellites. In this sense, it only partially evolved. It is this state of "suspended animation" that provides a unique opportunity for geophysical investigations.

2. The data

Three features of Iapetus' current state provide critical constraints for our models, which in turn yield information about Iapetus' past. These features are described in the next three sections.

2.1. Spin and orbit

Today, Iapetus' rotation period is 79.33 days and synchronous with its orbital period. Despinning to reach synchronicity is a result of tidal dissipation, a process that has occurred for all the regular jovian and saturnian satellites (except chaotic Hyperion). However Peale (1986) noted that Iapetus' synchronous spin was unexpected, because of its large semi-major axis ($D = 3.51 \times 10^6$ km, i.e., ~ 60 R_s) and the very strong (D^{-6}) dependence of the rate of despinning on distance to the planet.

Iapetus has a mean density of 1083 ± 13 kg/m^3 (Thomas et al., 2007). This means that it has a radiogenic bearing rock mass fraction of $\sim$20%, assuming the body is not porous. Iapetus' mean density indicates that it is most likely composed of water ice and chondritic carbonaceous chondritic material (from the kronian subnebula) with an enrichment in volatiles and, possibly, light hydrocarbons (Johnson and Lunine, 2005). Its composition and current orbital state are fully consistent with formation in its present place (Ward, 1981) as part of the saturnian system. (This will be discussed further in Section 5.)

Iapetus is "dynamically frozen" (to use a phrase from McKinnon, 2002). Its eccentricity is 0.0283, which suggests little dynamical evolution. Its orbital inclination is $\sim$7.49 degrees and its Laplace plane is inclined 14.968 degrees with respect to Saturn's equator.

2.2. Shape

Cassini images show that Iapetus is an oblate spheroid with a difference between its equatorial, a, and polar radii, c, of 35.0 ± 3.7 km (Thomas et al., 2007) (see Fig. 1). The equatorial radii a and b are the same to within 2 km, i.e., less than the uncertainty in the measurements. The residuals to limb fits over the wide range of longitudes and latitudes available, have an rms of 4.0 km (0.54% of the mean radius), and show, as does inspection of the images, that this shape is indeed an ellipsoid with superposed craterform topography. A symmetric difference of 34 km with such small residuals could not form by random cratering by large impacts. Nor is modification of a triaxial equilibrium form possible for two reasons. First, the difference of observed and predicted intermediate axes is over 26 km, a value not allowed by the measurement uncertainty. Second, to maintain an $(a - c)$ of 34.5 km with its slow rotation and observed mean density, Iapetus would have to be largely hollow with a high density, thin shell, clearly not physically plausible. The predicted $a - c$ for a homogeneous Iapetus is only $\sim$10 m for hydrostatic equilibrium for the current spin period, as illustrated in Fig. 1. Thus, Iapetus has the largest non-hydrostatic anomaly known for a satellite larger than 1000 km in radius, with the Moon being a distant second (Garrick-Bethell et al., 2006).

If Iapetus' interior is homogeneous, the observed figure is only plausibly explained as the shape for a body in hydrostatic equilibrium with a rotation period of $\sim 16 \pm 1$ h. A differentiated

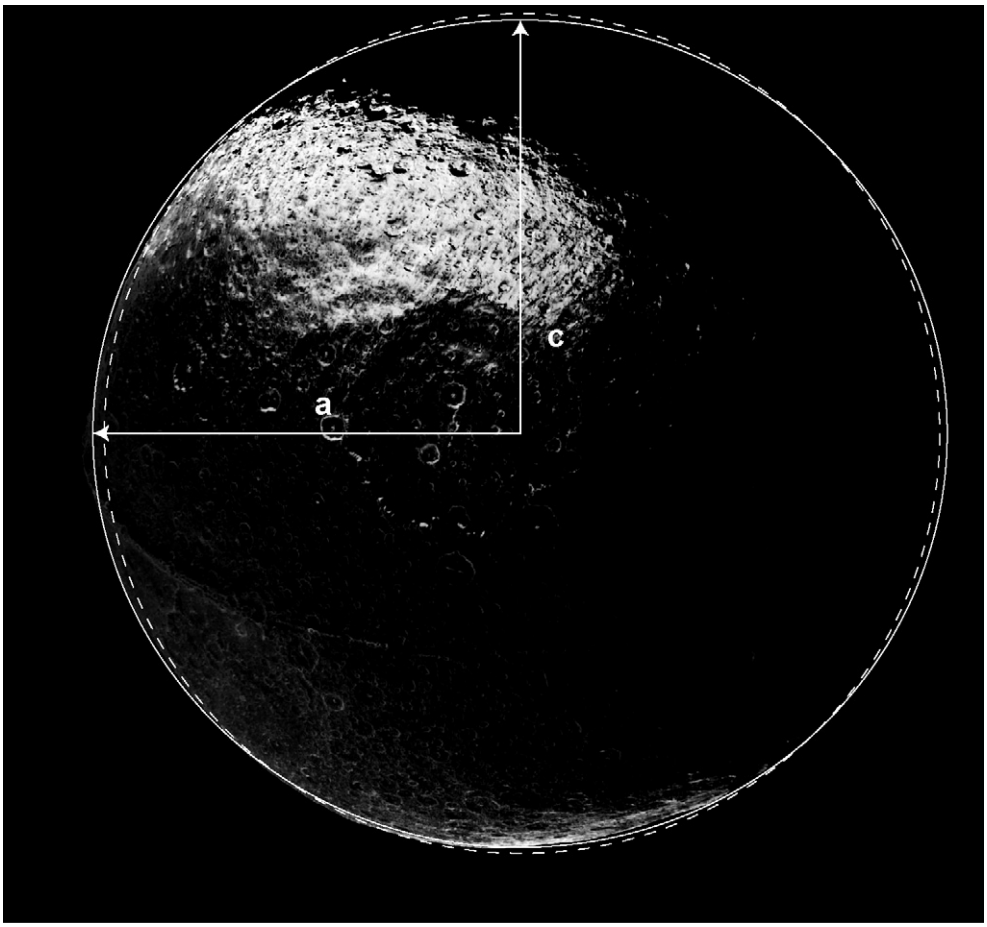

Fig. 1. Flyby picture of Iapetus by Cassini Imaging Sub-System (ISS) on December 31, 2004. The solid curve shows the large-scale shape of the satellite. The dashed curve indicates the shape the satellite would have if it were in hydrostatic equilibrium today. Given Iapetus' present rotation period and semi-major axis, a deviation from spherical of no more than 10 m is expected. The actual deviation is 33 km. At 9 o'clock on the limb of the disk the equatorial ridge is seen standing well above the other topography.

body with a core of density 3510 kg m^{-3} would need to have a spin period about 1.3 h less. In either case, this is far from the 79.33-day period.

This information suggests that Iapetus has a fossil shape that has been frozen when the satellite's lithosphere became strong enough to resist continued deformation at a time when the satellite was still despinning.

Similar scenarios have been proposed for the Earth (Mound et al., 2003), Moon (Lambeck and Pullan, 1980; Garrick-Bethell et al., 2006) and Mars (Zuber and Smith, 1997; Matsuyama et al., 2006).

This also suggests a constraint on the initial rotation period of the satellite. It should have been less than 16 h.

2.3. Equatorial ridge

A nother surprising feature of Iapetus' topography is a prominent equatorial ridge (Fig. 2) running most of the way around the equator. Where visible, this sits right on top of the equatorial bulge. The ridge is abundantly cratered, indicating that it is comparable in age to any of the terrains on Iapetus. It is clearly older than the large basins that overlap it. Anything this large, and this long, suggests global rather than local or regional control.

Data for estimating the volume of the ridge are sparse. *Cassini* observations (e.g., Fig. 2; Porco et al., 2005) cover only one side of the satellite. Denk et al. (2000) have detected this feature in *Voyager* data and conclude that it continues in the other hemisphere. They see the illuminated tops of equatorial peaks that lie on the nighttime side of the terminator as evidence for the continuation of the ridge. The ridge generally appears to be single, but in some places it is double or triple. The flanks are steep with slopes in some sections greater than 30 degrees. The volume of material involved in the ridge is very large. It spans at least half of the equator and is well developed over a length of ∼1600 km. A typical (triangular) cross-section has a base of 200 km and a height of 18 km, or a cross-sectional area of 1800 km^2, for a volume of $\sim 3 \times 10^6$ km^3. This estimate does not include any allowance for roots or folds.

We do not know how the ridge was formed. Porco et al. (2005) suggested that it is associated with Iapetus' despinning. This idea is based, in part, on the fact that the ridge is located at the equator. Denk et al. (2005) proposed that it resulted from volcanic activity. Giese et al. (2005) suggest that the morphology of the ridge indicates upwarping of the surface due to a

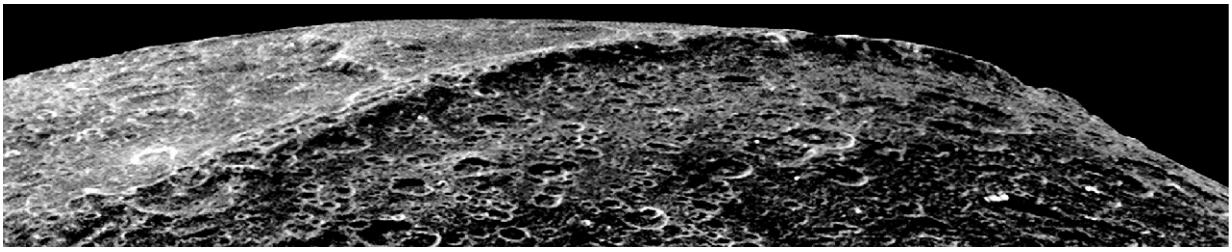

Fig. 2. Iapetus equatorial ridge as observed by Cassini ISS (Porco et al., 2005). Toward the left the ridge appears to have splayed into several approximately parallel components. The available images do not have enough detail to reveal how the ridge was formed.

tectonic (rather than a volcanic) event. We know little about the ridge's geological evolution.

If the ridge was created by folding, then its spatial wavelength of ∼200 km implies that the lithospheric thickness was ∼15–20 km, according to the relationship between the wavelength of folds and the thickness of the lithospheric shell that formed them (Turcotte and Schubert, 2002). Thus, the minimum lithospheric thickness required to preserve a 20-km high feature is about 15–20 km. However, the ridge could have been somewhat higher and subsequently relaxed to its present height. It is also possible that it resulted from faulting. Obviously, further imaging and interpretation are needed in order to better constrain the lithospheric thickness and the possible formation processes.

It should be emphasized that this feature is small compared to the global equatorial bulge. Removal of the ridge from limb data reduces the equatorial ellipsoid fit axes by only ∼1 km. The volume of the ridge is less than 5% of the equatorial bulge, and is clearly a surimposed form. Although the formation of the ridge and bulge may be related (see below), the significance of the oblate spheroid shape is independent of the formation mechanism and morphology of the ridge.

2.4. Objectives of this paper

The present paper reports our effort to find a scenario or scenarios that can explain both the present shape and rotational state of Iapetus, while being compatible with the preservation of the equatorial ridge. This scenario is based on the assumption that the shape's oblateness is a fossil from a period when Iapetus was spinning more rapidly than present.

Solving this problem requires simultaneous modeling of the thermal and orbital evolution of the satellite. Indeed, despinning, shape, and lithospheric evolution are functions of the thermal structure of the satellite (dissipation factor and Love number k_2). Thermal events determine the rotational and geological events leading to the present condition. For the satellite to despin while preserving its shape, it is necessary for the interior to still be dissipative after a lithosphere thick enough to support the equatorial bulge has developed. This provides constraints on the internal evolution chronology and suggests a period during which the body was spinning rapidly and its global rigidity was low enough for hydrostatic equilibrium to be achieved. Despinning must continue as the lithosphere becomes thick enough to freeze its shape, i.e., warm temperatures are reached in the deep interior of the satellite. We believe that external heat sources (such as impact energy) are not important since they would disrupt the overall ellipticity of the shape and lead to its relaxation, contrary to Iapetus' current state.

In the following sections we explain our models and test the possible scenarios meeting these requirements.

3. Internal evolution modeling

In this section we describe and justify the initial conditions used in the models. Then we explain the algorithms used for handling coupled thermal, dynamical, and geological processes.

3.1. Initial conditions

3.1.1. Composition

For the rock component we use an ordinary chondritic composition based on Wasson and Kalleymen's (1988) elemental abundances (Table 3). The corresponding density (used for the calculation of the rock-metal fraction) is 3510 kg/m^3. Radionuclide data for the long-lived radioactive isotopes (LLRI) are gathered in Tables 4 and 5.

Iapetus' icy component is assumed to be primarily water on cosmochemical grounds (e.g., Lewis, 1971), but it is likely that it also contains various volatile "contaminants." Carbon dioxide has been detected in small quantities by the Cassini Visual Infrared Mass Spectrometer (VIMS) (Buratti et al., 2005), but its origin is not established. Based on models of the properties and evolution of satellite-forming disks around giant planets, it is possible that ammonia is present at amounts relative to water of up to 11 wt% (Mousis et al., 2002). Recent measurements by *Cassini* RADAR (Ostro et al., 2006) identify ammonia as a contaminant that could explain RADAR observations at different wavelengths. The various "contaminants" may affect geophysical models (through the depression of the ice melting point)

Table 3
Initial isotopic abundances for the compositional model, ordinary chondrite, considered in this study

Property (unit)	Value
Density (kg/m^3)	3510
^{26}Al (ppb)	600
^{60}Fe (ppb)	22.5–225
^{53}Mn (ppb)	25.7
^{40}K (ppb)	1104
^{232}Th (ppb)	53.8
^{235}U (ppb)	8.2
^{238}U (ppb)	26.2

Table 4
Decay information for the LLRI (adapted from Van Schmus, 1995)

Element	Potassium	Thorium	Uranium	
Isotope	^{40}K	^{232}Th	^{235}U	^{238}U
Isotopic abundance (wt%)	0.01176	100.00	0.71	99.28
Decay constant (yr^{-1})	5.54×10^{-10}	4.95×10^{-11}	9.85×10^{-10}	1.551×10^{-10}
Half-life λ (Myr)	1277	14,010–14,050	703.81	4468
Specific heat production (W/kg of elements)	29.17×10^{-6}	26.38×10^{-6}	568.7×10^{-6}	94.65×10^{-6}

Table 5
Decay information for the SLRI (Kita et al., 2004; Tachibana et al., 2006; Chen et al., 2007)

Parent nuclide	^{26}Al	^{60}Fe	^{53}Mn
Daughter nuclide	^{26}Mg	^{60}Ni	^{53}Cr
Initial isotopic abundance	^{26}Al/^{27}Al = 5×10^{-5}	^{60}Fe/^{56}Fe = 0.1–1 $\times 10^{-6}$	^{53}Mn/^{55}Mn = 1–4 $\times 10^{-5}$
Half-life λ (Myr)	0.716–0.73	1.5	3.7
Specific heat production (W/kg)	0.146	0.068–0.074	0.027

by as much as at about 220 K in the case of CO_2 and 176 K in the case of NH_3 (see Section 4.4). Other possible contaminants, such as methane (CH_4), will not measurably lower the melting point but could—through the formation of clathrate hydrate—alter the thermal conductivity of the interior. The resolution of these issues is not possible with the current laboratory data. Thus, we use the properties of pure water and then discuss how the results might be perturbed by other volatiles.

3.1.2. Physical structure

Porosity can have a significant effect on the internal evolution of a satellite, affecting the relationship between the bulk and the mineralogical densities, the strength of the material, and the thermal properties. Porosity varies with time due to thermal evolution.

When hydrostatic pressures exceed the strength of ice, compaction takes place due to brittle facture and reorganization of the material (e.g., Durham et al., 2005). Laboratory measurements by Durham et al. (2005) on pure water ice show that porosities of up to 15% can be sustained at pressures up to 150 MPa when the temperature is less than 120 K. Such a situation is encountered in Iapetus at the end of accretion (max pressure is ∼125 MPa). These conditions are realized at some time in most medium-sized satellites. Porosity decreases with depth. There is an abrupt change between a few MPa and 10 MPa, due to brittle fracture and reorganization of the material. For pressures of less than 1 MPa the porosity can be as large as 40% (e.g., Durham et al., 2005). Under suitable conditions, especially temperature, ice creep and sintering produces further structural evolution, and porosity becomes vanishingly small. Leliwa-Kopystynski and Kossacki (1995) have recognized the importance of for these mechanisms. For example, the presence of rocky material impedes the decrease of porosity by compaction. On the other hand, these laboratory experiments indicate that the presence of NH_3 (and perhaps other "contaminants") increases ice creep and compaction.

Porosity has consequences not only for the structural evolution of the satellites (and resulting thermal conductivity, see Section 3.2.1), but also has a direct effect on interpreting the measured densities. This has consequences for assessing the radionuclide content, and thus upon thermal evolution. While it is possible to determine the evolution of porosity with time, and quantify the density changes associated with this effect, there is a reciprocal coupling between porosity and the ice-to-rock ratio (i.e., the specific concentrations of radionuclides). In order to set the correct initial ice-to-rock ratio the present porosity of the body must be known. However, in many cases the porosity today for a given model is determined by the relative abundance of rock (i.e., radioactivity) initially present in the model and how much porosity it destroyed by "baking." Therefore, in this regard, we must be careful that our models are self-consistent and it may be necessary to use the model iteratively in order to converge upon a solution for porosity.

3.1.3. Initial dynamical parameters

The initial rotation periods of the giant-planet satellites are not known. Data available for spin rates of asteroids (Dermott and Murray, 1982) range from 5 to 12 h. The asteroidal spins are unlikely to have been slowed by tidal dissipation as can occur for satellites. Thus these statistics give a better indication of reasonable initial spin rates for satellites. Conservation of angular momentum in the satellite-forming gas/dust disk suggests that Iapetus should have followed this statistical trend and accreted like other satellites, with a rapid initial spin period of a few hours (Pravec et al., 2002; Lissauer and Safronov, 1991). From Roche's limit, we know that the initial period for Iapetus, T_0, cannot be less than 3.8 h.

Our assumption that Iapetus was despinning from a high rate and had a spin rate of ∼16 h when its present shape was frozen is consistent with the considerations in the previous paragraph.

We assume a 7-h initial rotation period for all of the models in this paper. It turns out that as long as this initial period is less than 16 h, its exact value has little effect on the calculations presented here.

Iapetus has a high eccentricity, $e = 0.0283$, and is so far away from Saturn that it suggests that the body is "tidally frozen" (McKinnon, 2002). This is further indication that the

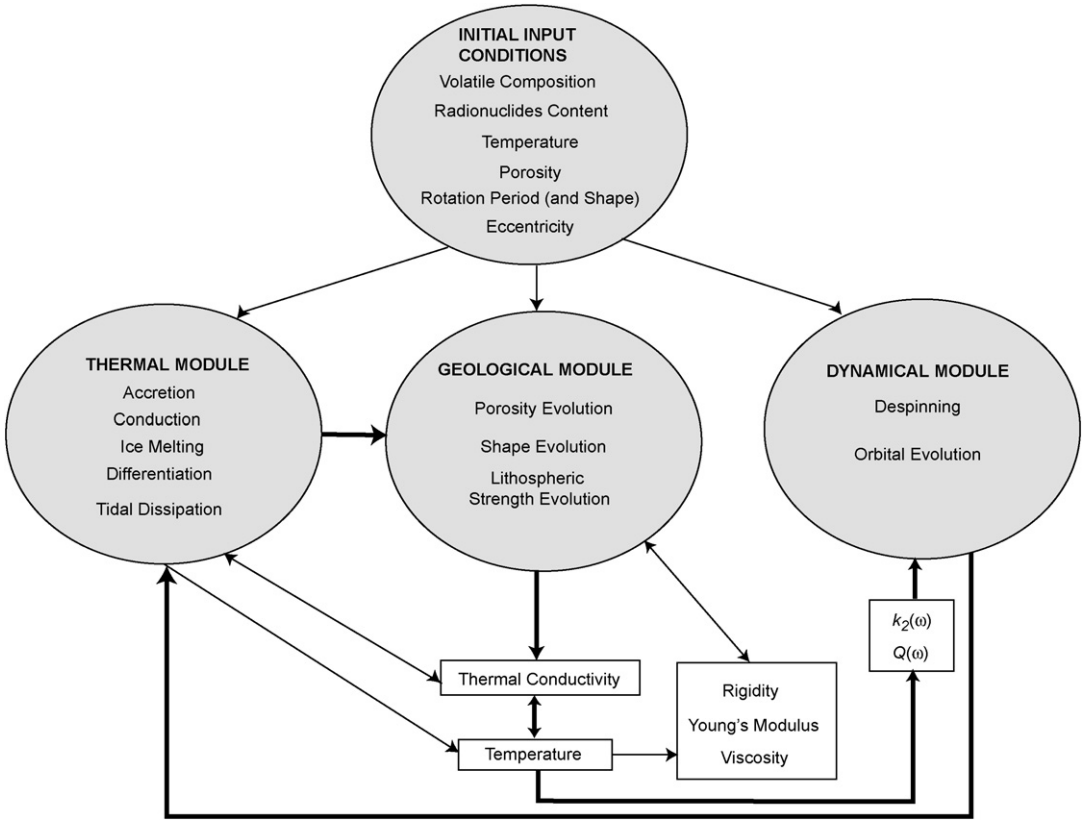

Fig. 3. Schematic diagram of the calculation scheme. The connections between the modules and the flow of some of the parameter values are shown.

object is old and underwent relatively little tidal dissipation over most of its history.

3.1.4. Initial shape

Shape is treated as a dependant property. We compute Iapetus' rotational oblateness using Chandrasekhar's (1969) formulation. The theoretical shape, as a function of spin period and mean density for a homogeneous object, is a MacLaurin spheroid. This is a reasonably accurate representation for spin periods as low as a few hours. For both homogeneous and two-layer models, we employ numerical methods modified from Thomas (1993) and Thomas et al. (2005) that determine equilibrium shapes, or departure there from, to accuracies of 1.3×10^{-4} for shapes appropriate for spin periods down to 10 h, and somewhat less accurately for the more elongate forms at faster spin rates. The equatorial and polar radii as a function of the rotation period are presented in Fig. 4.

3.1.5. Time of formation

Short-lived radioactive isotopes are known to be present in the early Solar System on the basis of meteoritic analysis. Their presence is inferred primarily from their stable daughter products in some of the oldest refractory, calcium–aluminum inclusions (CAIs), found in carbonaceous meteorites (Wasserburg and Papanastassiou, 1982). The decay of SLRI, such as ^{26}Al, ^{60}Fe, and ^{53}Mn has been proposed to be potentially important for the evolution of the early Solar System (Urey, 1955), and for the thermal evolution of asteroids and icy bodies (Prialnik and Bar-Nun, 1990). The initial concentration of ^{26}Al/^{27}Al is assumed to be the "canonical" maximum value ($C_0 = 5 \times 10^{-5}$) (Wasserburg and Papanastassiou, 1982). For the initial ^{60}Fe/^{56}Fe isotopic ratio we have taken an order of magnitude, range based on numbers in the literature (see Chen et al., 2007 for a review), i.e., 1×10^{-7}–1×10^{-6}. The lower bound is based after Tachibana and Huss (2003) and the upper bound is set based on measurements by Mostefaoui et al. (2005) and Tachibana et al. (2006). The initial concentration of ^{53}Mn/^{53}Cr ranges between 1 and 4×10^{-5} (Kita et al., 2004). Note that the contribution of ^{53}Mn to the total heat budget is significantly less by two orders of magnitude than the contributions of ^{26}Al and ^{60}Fe.

Work in progress (McKeegan et al., 2006) has identified CAIs in samples from the comet *Wild 2* obtained by the *Stardust* mission. This is the first evidence that CAIs were present in the outer Solar System. However, at this time it has not been shown that the concentrations of the SLRI obtained from the analysis of meteorites apply to the outer Solar System (as predicted by the supernova model). Some lateral heterogeneities in ^{53}Mn and ^{26}Al concentration have been identified by Gounelle and Russell (2005a, 2005b). This is presently a matter of debate as it depends on the origin of the elements and the spatial scale of the heterogeneities (the scale sampled by the CAIs-chondrules vs scale of planetary systems).

As we investigate the potential effect of SLRI on our models, we use the formation of CAIs as our time reference. The initial level of SLRI activity in Iapetus is set by the time at which Iapetus accreted. For our models of Iapetus the thermal effect

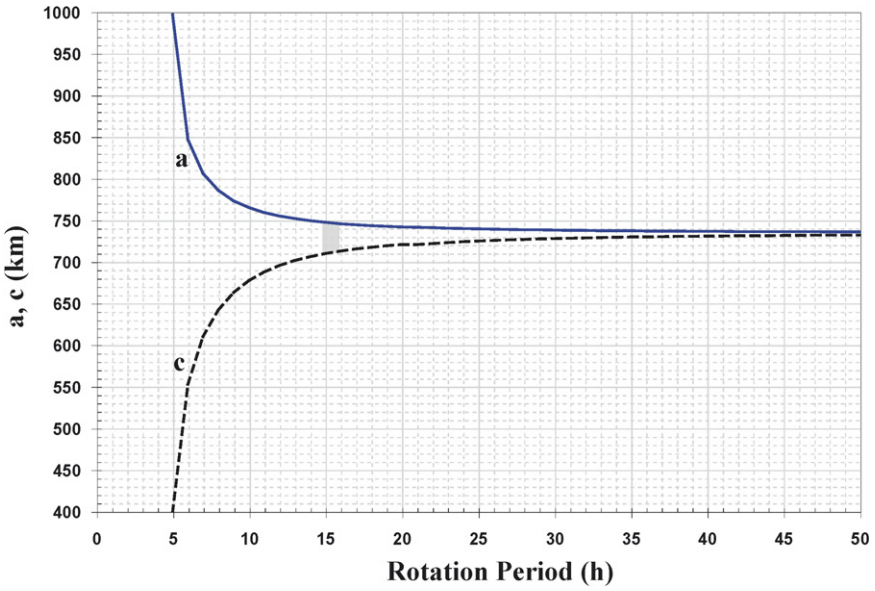

Fig. 4. Equatorial and polar radii for a satellite with a mean radius of 735 km, as a function of the rotation period.

of SLRI becomes insignificant when the time of formation becomes larger than ∼6 Myr after CAIs.

3.1.6. Initial temperature

The initial temperature is a function of (a) the temperature of the accreting planetesimals, labeled T_i and (b) accretional heat from the kinetic energy of the planetesimals. The temperature of the accreting planetesimals is related to the composition, temperature and pressure of the subnebula at Iapetus' distance from Saturn. We consider $T_i = 90$ K as a reasonable upper bound corresponding to the temperature in equilibrium with sunlight at Iapetus 4.5 byr ago, when the luminosity of the Sun was about 70% its present value (Endal, 1980).

We model accretion following Squyres et al. (1988). The parametric ratio of mechanical energy turned into heat, h_a, can range from 0.1 to 1.0. The higher value is justified by the possible formation of a greenhouse during very rapid accretion (Lunine and Stevenson, 1982). We treat accretion as rapid with respect to SLRI decay (Mosqueira and Estrada, 2005) and as a result we do not consider the effect of SLRI on the initial temperature profile.

Accretion does not contribute significantly to warming the interior because most of its heat is deposited close to the surface where it is conducted upward and then radiated to space (Squyres et al., 1988). The maximum increase in accretion temperature ΔT_a ranges from $\Delta T_a = 10$ K for $h_a = 0.1$ to $\Delta T_a = 130$ K for $h_a = 1$. Halfway down in Iapetus, this temperature increase is $\Delta T_a = 2$ K for $h_a = 0.1$ and $\Delta T_a = 30$ K for $h_a = 1$. Thus, accretional heat cannot raise the internal temperature to the ice melting point, unless ammonia or other "contaminants" are mixed with the water. If $h_a > 0.6$, accretional heat can play a role in decreasing the porosity of the satellite's outer layer. These assumptions are consistent with previous studies of icy satellite accretion (e.g., Ellsworth and Schubert, 1983). We test different values of h_a in our models, as will be discussed later.

3.2. Algorithms

Our coupled thermal evolution model is comprised of three "modules." The relationships between these modules are illustrated in Fig. 3. The thermal module calculates the one-dimensional temperature field and the resulting heat flows. The dynamical module calculates the change in the rotation rate and the eccentricity. Material properties are updated at each time step based on the current temperature and dynamical state. The geologic module keeps track of size, shape (e.g., changes in volume and surface area) and structure. Temperature is the parameter common to the different modules. The radial grid size is 5 km. The time step is 10^4 yr.

3.2.1. Thermal module

The thermophysical module accounts for all of the known sources and sinks of energy. It calculates the one-dimensional temperature field and the resulting heat flows and phase changes. For example, the models take into account tidal heating resulting from despinning (after Burns, 1976) and subsequent eccentricity decay (after Peale, 1999). We consider one-dimensional models corresponding to the situation at the equator. Details on the equations used in the algorithm are presented in Appendix A. Two-dimensional thermophysic–dynamical evolution models are discussed in Section 5.

Heat transfer first occurs by conduction (e.g., Hillier and Squyres, 1991; Appendix A). We present conductive models under the assumption that subsolidus convection could not take place before despinning is complete. We address in the discussion (Section 5) the arguments supporting this scenario.

Differentiation is modeled as a quasi-instantaneous process (short compared to time scales related to heat generation and heat transfer) that starts when the melt fraction becomes larger than 2% (De La Chapelle et al., 1999). This assumption relies on the fact that fluids migrate quickly in comparison with the other physical processes modeled in the present study.

Table 6
Thermal parameters as a function of composition and temperature (after McCord and Sotin, 2005) (x_s is the silicate mass fraction)

	Silicate	Ice	Mixture of ice and silicates
Thermal conductivity (k in W/m/K)	4.2	$0.4685 + 488.12/T$	$f_s k_S + (1 - f_s)k_I$
Heat capacity (C in J/kg/K)	920	$185 + 7.037T$	$x_s C_S + (1 - x_s)C_I$

Thermal parameters (thermal conductivity and specific heat) are temperature-dependent (see values in Table 6). Porosity can have a significant effect on the thermal conductivity (see McKinnon, 2002 for a review). The effect is difficult to assess accurately as it is a function of the microstructure of the material. Indeed, depending on porosity, the thermal contacts between the grains will be more or less efficient in transferring heat. We follow the approach of McKinnon (2002) who defines two bounds for thermal conductivity. The upper bound is a function of the *effect of void volume fraction* on the equation of the thermal conductivity of a mixture of ice, silicate, and voids. The lower bound is a rough assessment of the effect of *structural arrangement* and grain contact. McKinnon (2002) notes that lack of knowledge of this parameter means that we should consider the effects of a decrease in thermal conductivity of a rock-ice-void mixture by up to one order of magnitude. However, some constraints on this factor are available from laboratory measurements and theoretical studies of grain assemblages. Ross and Kargel (1998) show that this structural effect is a function of pore size and shape. From their Fig. 5 we infer that in the upper, high porosity layer (i.e., regolith) conductivity can be decreased by a factor of about 10 with respect to solid ice. This roughly corresponds to laboratory measurements performed on lunar regolith samples (Langseth et al., 1976) and telescopic constraints on the values for Europa's surface conductivity selected by Matson and Brown (1989). In the interior, where the porosity is in the form of closed pores, this thermal conductivity is lessened at most by a factor of two.

Thermal conductivity is also a function of the composition. Ross and Kargel (1998) and Lorenz and Shandera (2001) have measured thermal conductivity for different mixtures of water and ammonia or methane. Lorenz and Shandera (2001) show that when 15% ammonia is mixed with ice, the thermal conductivity is about 1.5 $\mathrm{W\,K^{-1}\,m^{-1}}$, and is barely dependent on temperature. This value is 2 to 3 times lower than pure ice thermal conductivity. Thus ammonia can play an insulating role especially at very low temperatures when solid water ice thermal conductivity can be as large as 4.5 $\mathrm{W\,K^{-1}\,m^{-1}}$. There are few data available for mixtures containing less than 15% ammonia.

3.2.2. Dynamical evolution module

This module calculates changes in the spin of Iapetus as it proceeds along its evolutionary track. For most of the time, and before synchronicity is reached, this amounts to adjusting the instantaneous rate at which despinning takes place due to dissipation within the body. There is also a small increase in spin during the times when the models experience a decrease in porosity, thus in volume. This effect is relatively small compared to other sources of modeling uncertainty and is not included in the present evolutionary calculations.

When the body has despun, tidal friction is then employed to evolve the orbital semi-major axis and eccentricity.

Details on the equations used in the algorithm are presented in Appendix B.

3.2.2.1. Despinning (Appendix B.1) The evolution of Iapetus' spin (ω, in rad/s) as a function of time, t, is governed by

$$\frac{\mathrm{d}\omega}{\mathrm{d}t} = -\frac{3k_2(t)GM_\mathrm{p}^2 a^5(t)}{C(t)D^6 Q(t)}, \tag{1}$$

where G is the universal constant of gravity, M_p Saturn's mass, a Iapetus' equatorial radius, C the polar moment of inertia, and D the semi-major axis. The dissipation factor Q and the tidal Love number k_2 are functions of the frequency-dependent viscoelastic properties of the satellite and thus vary as a function of time. The difficulty in despinning a distant satellite results directly from the strong (inverse sixth power) dependence on D in Eq. (1).

A major difference between our present study and previous work is that the time-dependent parameters are recomputed for each computational time step. This is especially the case for Q and k_2 that are functions of the tidal (excitation) frequency ω.

Parameters that are well constrained (well known or derived from the combination of known parameters) are M_p, G, a, and C. Regarding D, a small amount of semi-major axis evolution would not matter much because Iapetus is so far from Saturn. Parameters that are the most influential in determining the spin history, but also are the least constrained, are the initial rotation period T_0, the dissipation factor Q, and the tidal Love number k_2.

3.2.2.2. Eccentricity evolution (Appendix B.2) There is little constraint on the tidal parameters k_p and Q_p for Saturn besides indirect constraints based on Mimas' orbital evolution, i.e., $k_\mathrm{p} = 0.341$ and $Q_\mathrm{p} = 1.6$ to 6×10^4 (Gavrilov and Zharkov, 1977; Peale et al., 1980; Dermott et al., 1988). The eccentricity damping due to the effect of Iapetus on the planet is $\sim 10^{-26}\ \mathrm{s^{-1}}$ and the contribution to the eccentricity damping due to internal dissipation in Iapetus is $\sim 10^{-19} \times k_\mathrm{s}/Q_\mathrm{s}\ \mathrm{s^{-1}}$. Whether the ratio $k_\mathrm{s}/Q_\mathrm{s}$ is maximum (i.e., $k_\mathrm{s}/Q_\mathrm{s} = 1$) or minimum (i.e., $k_\mathrm{s}/Q_\mathrm{s} = 0$), the time needed for the eccentricity to evolve is much larger than the age of the Solar System, unless the initial eccentricity is very close to its present value. Similar reasoning based on Peale (1999) indicates that the semi-major axis evolution has been negligible over Iapetus' lifetime. Thus, little dynamical evolution has taken place post-despinning and Iapetus' present semi-major axis and eccentricity are indicative of its initial state.

3.3. Geological module

The geological module calculates size, shape and structure during the evolution of Iapetus. Calculation details are presented in Appendix C.

The different processes handled by it are functions of the conditions of the mechanical lithosphere, i.e., of the temperature distribution and mechanical properties. The latter are addressed in Section 3.4.

Two processes act to change volume: phase changes and porosity decrease. Also volume redistribution occurs during the change in shape as Iapetus despins and becomes less of an oblate spheroid. This is always accompanied by an adjustment of the surface area, which can result in tectonic processes such as folding, faulting, etc., that are functions of the properties of the mechanical lithosphere (although these mechanical effects of surface area change are not modeled in the current version of the program). Also, the shape surface area evolves as a function of the spin period. Details of the calculation are presented in Appendix C. Values of a and c are plotted as a function of rotation period in Fig. 4.

We compute the evolution of internal porosity when conditions are suitable for ice creep. Porosity removal is computed after Nimmo et al. (2003). We use the compaction rules developed by Leliwa-Kopystynski and Kossacki (1995, 2000). They have different rules depending on composition, silicate mass fraction, and ammonia content (or other "contaminants").

3.4. Material rheology

The rheological properties of the material, i.e., rigidity and viscosity, are a common thread between the different processes investigated. For despinning, Eq. (1), this is accomplished through the degree-two tidal Love number k_2, and dissipation factor Q. For the assessment of the strength to preserve the large-scale shape over the long run, it is through Young's modulus (Eq. (2)) and the relaxation time (Eqs. (4) and (5)).

3.4.1. Rigidity

Rigidity μ is a material property that is a function of composition, temperature, and structure. It is formally defined as the real part of the shear modulus μ.

In practice we use Young's modulus E, which is directly related to the shear modulus μ by

$$E = \frac{2\mu}{1+\nu}, \tag{2}$$

where ν is Poisson's ratio taken as its average value for icy materials (i.e., $\nu \sim 0.33$).

Young's modulus of solid water ice is well known for temperatures higher than 250 K. Nimmo (2004a) showed agreement, within a factor of two, between laboratory measurements and field measurements obtained for terrestrial glaciers. Nimmo (2004a) proposed $E = 9$ GPa, as a representative value for Young's modulus for water ice at temperatures greater than 250 K.

Fewer data are available for the situation of most medium-sized icy satellites, in which the temperature can be as low as 40 K. We use Nimmo's (2004a) value as an upper bound for computing the mechanical lithospheric thickness required for supporting nonhydrostatic topographic anomalies. [Note: there are several values of E in the literature (e.g., Lorenz and Shandera, 2001)].

Durham et al. (1998) and Lorenz and Shandera (2001) have also measured the elastic modulus for water–ammonia mixtures. For 16% ammonia mixed with water, assuming that the corresponding Poisson's ratio is ~0.33, Young's modulus varies between 9 GPa at 100 K and 9 MPa at 170 K. Data for other mixtures are scarce. Increasing the amount of rock tends to increase the rigidity (e.g., Durham et al., 1989).

Porosity also weakens the material. This is particularly so when the microscale rigidity of the material is applied to cases where we need to calculate the intrinsic rigidity of the satellite. This satellite-wide-scale rigidity can be affected by the development of faults, open pores, closed pores, and other effects that greatly weaken the lithosphere. Porosity can decrease rigidity by up to 50% (e.g., Berryman, 1995) depending on the size and organization of the pores. Measurements on laboratory-prepared, porous, "sea" ice by Cole (1998) show a relaxation of compliance and a rigidity decrease of one order of magnitude when the porosity increases from 1 to 15%.

3.4.2. Viscosity

Viscosity plays significant roles in tidal dissipation and in convection, and hence is important in calculating despinning rates. Its value is also critical for starting convection. Viscosity is primarily a function of temperature, but is also dependent on other parameters such as stress, grain size, partial melt, and impurities. While the latter parameters are less important in determining the value of viscosity, they can play a role in starting convection as discussed in Section 5.1.2. For the present calculation we use an Arrhenius' law to describe the viscosity η as a function of temperature (after Deschamps and Sotin, 2001):

$$\eta = \eta_0 \exp\left[Q(1/T_\mathrm{m} - 1/T)\right] \tag{3}$$

with η_0 the reference viscosity at the ice melting temperature T_m.

Further discussion of the link between tidal dissipation and convection is found in Section 5.1.2.

3.4.3. Frequency-dependent viscoelastic behavior

The theoretical value of k_2 for an undifferentiated elastic Iapetus is 0.001. We take this as our lower bound for k_2. It is possible to increase the value of k_2 by decreasing the intrinsic rigidity of the body. This can be done, for example, by global-scale fracturing, say by a massive impact. This has been studied for the Moon (Pritchard and Stevenson, 2000). However, for Iapetus such shattering of the lithosphere runs counter to the necessity of building a stiff, strong lithosphere capable of supporting large-scale topography. To support such topography, a low rigidity would require an implausibly thick lithosphere, approximately thirty times thicker than for the non-fractured case, greatly exceeding the radius of the satellite. To be consistent with this constraint, the rigidity cannot vary by more than a factor of three from the theoretical value for solid ice.

Commonly used viscoelastic models have different responses to frequency, and different mechanisms for dissipation. We use Maxwell rheology in this study. This model is primarily dependent upon temperature and is not very dependent upon structural effects (Zschau, 1978).

At the low temperatures (<200 K) in the early history of the satellite, a Maxwell model tends to greatly overestimate the dissipation factor whereas other models might be more accurate (Tobie et al., 2005). Other rheology models that were established for the Earth include Burgers (e.g., Reeh et al., 2003) or Cole (Cole, 1995, 1998), which involve a structural component and several relaxation times. These models globally agree with the Maxwell models for temperatures greater than 240 K. However there are not yet enough data available for extrapolation to Iapetus' cold temperatures to be able to use any of these models. Recent studies have shown that it is possible to have materials with high attenuation/high rigidity (McCarthy et al., 2006), although insufficient data are available to incorporate materials with such properties into our models. It has been suggested that the ice dissipation factor at temperatures below the ice creep temperature should not be greater than 10^4 (Showman et al., 1997). We use this value as an upper bound to avoid severely overestimating Q due to the characteristics of the Maxwell rheology at low temperatures.

3.5. *Summary—constraints on the algorithms*

The output from each of our model runs is tested to see if it despins Iapetus to synchronous rotation. At the time the rotation period is 16 h the lithosphere is tested to see if it has sufficient thickness and strength to support the 16-h shape. We use a simple criterion to test whether a model can support the equatorial bulge over the long term. We apply the equations in Appendix C.1 in a static way, i.e., we do not consider possible relaxation while the lithosphere is thickening. The validity of this is discussed in Section 5.3. For supporting a 13-km topographic excess at the equator (i.e., difference between hydrostatic and observed radius), it is necessary that the lithospheric thickness be more than 230 km for a Young's modulus of 9 GPa. This is a lower bound because it is for a pure water-ice lithosphere. If the lithosphere is porous, then this minimum lithospheric thickness must be increase in order to compensate for the decrease in material strength.

4. Iapetus model results

Our models differ from earlier ones in the published literature via one or more of (1) temperature-dependent parameters, (2) the presence of ammonia (or other "contaminants"), (3) an initial porosity profile (Section 3.1.2), and (4) SLRI.

We assume that the conditions are such that convection does not start. If it did, it would efficiently remove internal heat. If convection starts before despinning can be achieved, then the modeling problem is not solvable. We discuss interior conditions under which our approach is valid in Section 5.1.2. As a result we present models whose heat transfer is governed by conduction.

For each case we present, we will discuss the resulting temperature and porosity as a function of equatorial radius, and time after accretion (Figs. 5–8). Temperature contours are

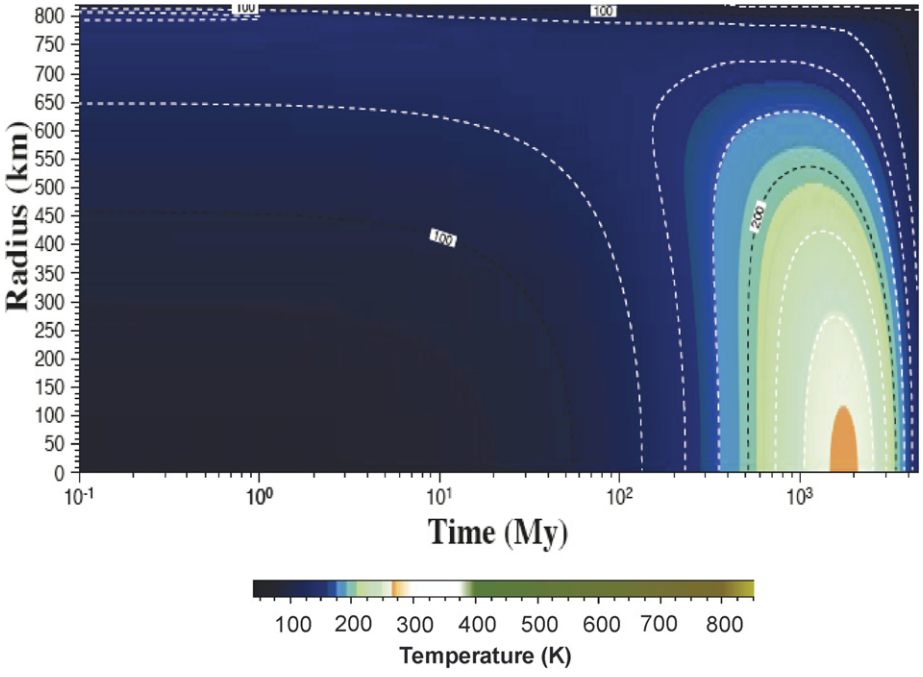

Fig. 5. Thermal evolution for a conventional model of Iapetus. We have updated the parameters in the Ellsworth and Schubert's (1983) model using current data for ice. The composition is pure water ice and rock with no initial porosity. The heat sources are accretion and the decay of long-lived radioactive isotopes (LLRI). Temperature is plotted as a function of equatorial radius and time (on a log scale) since accretion. The time at the extreme left is the start of the model. The time at the extreme right is the present. The temperature contours are every 25 K. Numerical call-outs are temperature in Kelvin. The color scheme indicates geophysically significant temperatures. This model serves as a baseline with which to compare the other models presented in this paper.

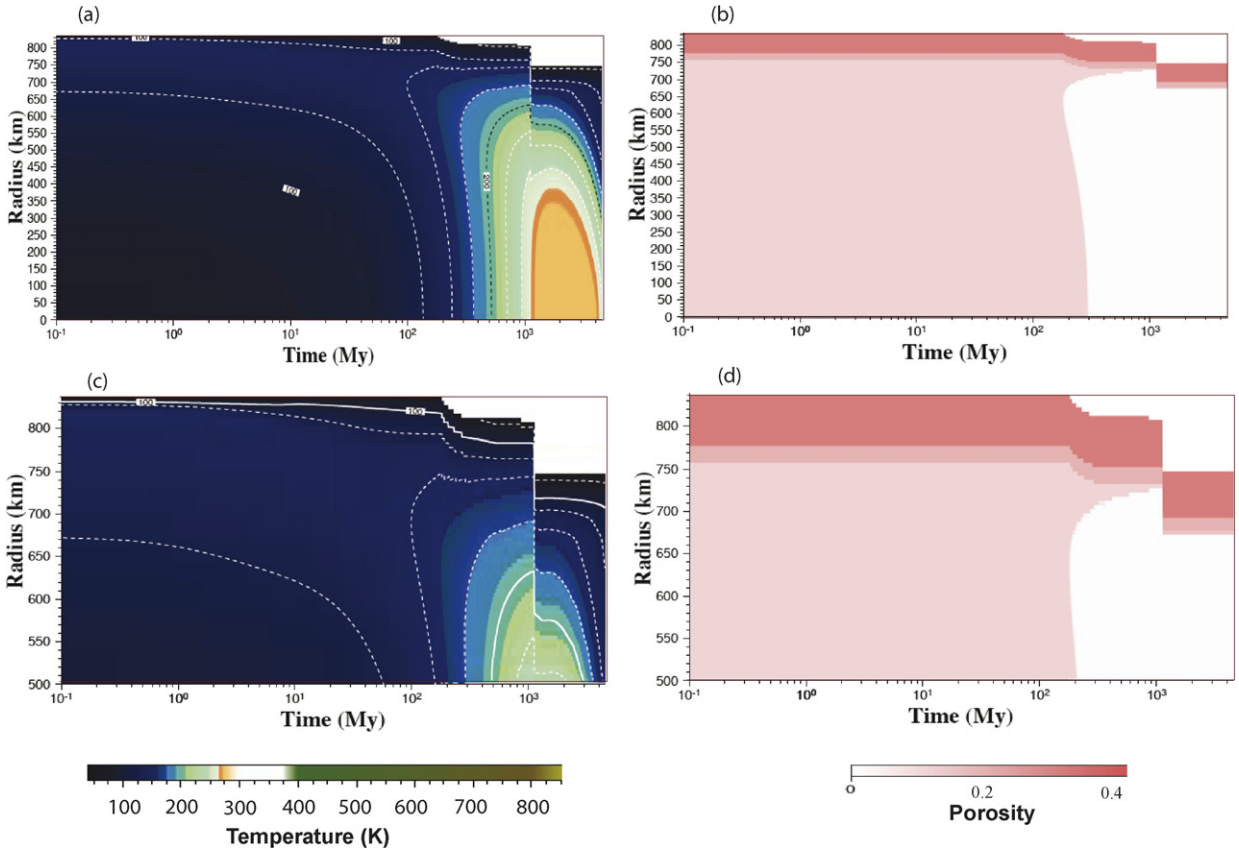

Fig. 6. Same model as in Fig. 5 but with the addition of an initial porosity profile based on Durham et al. (2005) and Kossacki and Leliwa-Kopystynski (1993). (a) Thermal evolution plot (as in Fig. 5); (b) the corresponding porosity evolution; (c) enlargement of the temperature plot for the outer 350 km, and (d) the corresponding enlargement for the porosity evolution. Note the adjustment of radius as the porosity collapses.

drawn every 25 K, and important temperature regions are color-coded (with a nonlinear, recursive palette). The decreases in the radius as a function of spin evolution and porosity are represented by the decreasing ordinate range of the data. A magnified view of the outer shell is also featured in Figs. 6 and 7. The plot of the global dissipation factor versus time is shown in Fig. 9. We now discuss these results.

4.1. Conventional model

We take the Ellsworth and Schubert's (1983) model as representative of the published state of the art in modeling Iapetus with LLRI heat sources. We apply to it the updated parameters as just described in Section 3. We call this updated version the *conventional model*. Comparison with this model gives us a way to check the accuracy of our calculations. It also provides a frame of reference within which to compare our new results with previous discussions.

The assumption that convection does not start allows us to assess the maximum temperature reached in the interior of the conventional model. The resulting thermal evolution is displayed in Fig. 5. We observe that the maximum temperature reached inside the body is less than the water ice melting point for most of the evolution. Although the results are qualitatively similar to Ellsworth and Schubert (1983), the high thermal conductivity of ice at low temperatures used in our model results in colder temperatures. Temperatures are not high enough for starting and sustaining significant evolution of the satellite. Under such conditions, despinning is not even triggered, and hence models of this type cannot explain the present state of Iapetus.

4.2. Model with long-lived radiogenic isotopes (LLRI) and initial porosity

The initial conditions for this model differ from the *conventional model* by starting with a porosity profile (Fig. 6, upper right panel). At ∼200 Myr after the start of the model, deep seated porosity begins to collapse as a result of an increase in the internal temperature and the radius decreases. At ∼1.1 Gyr the temperature reaches the ice melting point and rapid despinning takes place. The rotation period at the time of despinning is between 13 and 17 h (see Section 5.1.2 for more discussion). At this stage, porosity remains high in the outer 80 km of the satellite. The internal temperature is at the water ice melting point out to a radius of 350 km. That creates the conditions needed for completely despinning Iapetus. This is an interesting result because the despinning is, in effect, brought about by the insulating action of porosity. However the mechanical lithosphere, whose base is defined as the water-ice creep temperature, is at a depth of only ∼70 km, and its rigidity is significantly less that of solid ice due to its porosity. This makes it too weak to support the 16-h hydrostatic shape. In such a situation the equatorial bulge will relax by ∼6 km (if porous material rigidity is

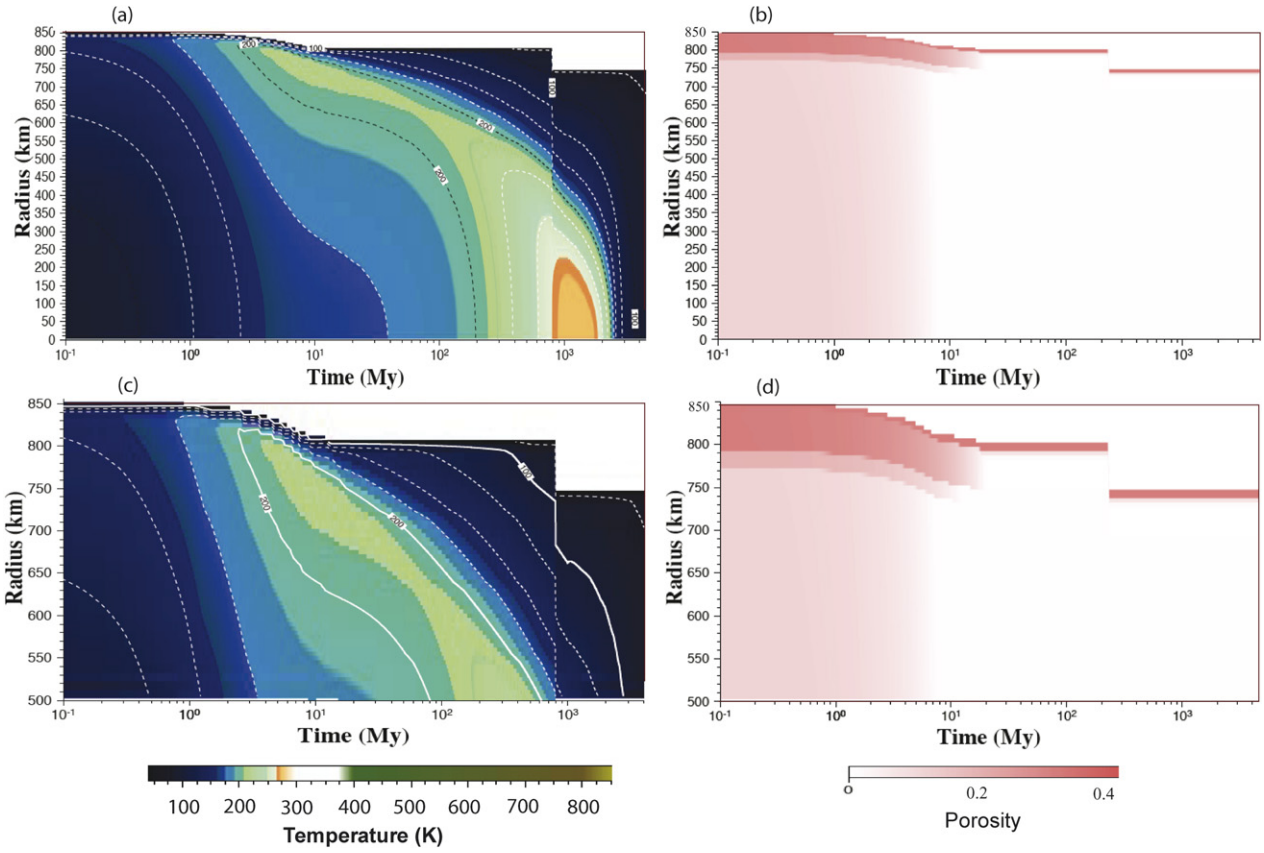

Fig. 7. Same model as in Fig. 6 but with an initial complement of short-lived radioactive isotopes (SLRI) appropriate for accretion 3 Myr after the formation of the calcium aluminum inclusions (CAI). (The surface steps between 4 and 10 Myr after the model formed are an artifact due to the granularity of the calculation.)

decreased by 50%) up to full relaxation (if rigidity is decreased by one order or magnitude with respect to porous ice). Also note that since this model results in remnant porosity today, it is necessary to iteratively update its composition to properly balance porosity, rock, and ice fractions. The zero-porosity equivalent density of this model is 1150 kg/m^3, which gives a rock mass fraction of 0.25.

In summary porosity and LLRI allow Iapetus to despin, but at the time of despinning the crust would be weak and the current shape would be partially to fully relaxed to the 79.33-day spin period.

4.3. Porous model with short-lived radioactive isotopes (SLRI)

This model differs from that of Section 4.2 by including SLRI in its early history (Fig. 7). As a first example, we take an initial concentration of ^{60}Fe/^{56}Fe equal to 1×10^{-6}, $h_a = 0.5$, and a time of formation after CAIs, $t_{0\text{-CAIs}}$, of 3 Myr. This choice of parameters is based on a previous estimate by Castillo et al. (2005) of a starting time, which would lead to despinning.

Rapid heating from SLRI results in the early collapse of porosity, about 1.5 Myr after the end of accretion. This collapse starts from near the surface due to the initial effect of accretional heat. Most of the porosity, except for that in the outer ∼5 km of the regolith, is removed by ∼15 Myr. During this period the combined contribution of accretional heat and SLRI results in thinning the lithosphere to a thickness of less than ∼20 km. After the porosity has been removed the thermal conductivity approaches the value of conductivity for solid ice. The lithosphere continues to cool and thicken while temperatures at depth continue to increase due to LLRI.

Conditions for despinning are reached at ∼800 Myr after formation. Despinning is a rapid process achieved in a few My, when the rotational period reaches ∼16 h (see Fig. 9). At that time the porosity is negligible and the lithosphere has a thickness of ∼240 km. The total relaxation of the lithosphere following despinning is less than 2 km. Some differentiation may occur when temperatures at depth reach the ice melting point.

In summary, models with porosity and SLRI are successful models, which allow full despinning and are theoretically able to support the non-hydrostatic topographic anomaly.

4.4. Models with ammonia

Ammonia is a potential contaminant for Solar System ices. It can play a significant geophysical role since it can depress the melting point of the water–ammonia mixture. At the present time, the amount of ammonia that accreted in Iapetus is poorly constrained as is the amount needed to produce full differentiation. This problem has not been studied in detail. The issues involved are how does ammonia–water liquid percolate through a water–ice matrix, and how does the rock separate from the ice, all at a time when the water ice is just approaching a temperature at which creep can start. Note that there is a major differ-

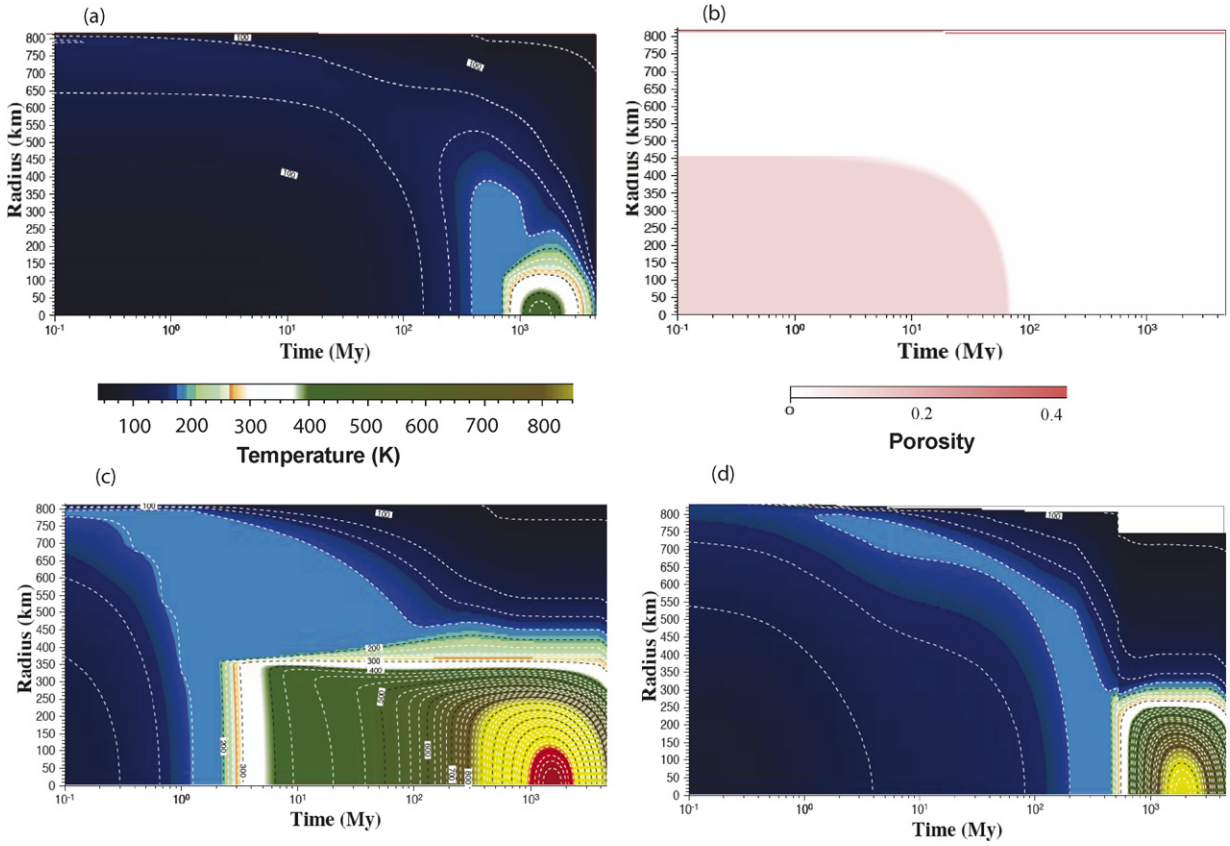

Fig. 8. Same models as shown in Fig. 6 but with enough ammonia to produce early melting and differentiation. (a) Thermal model without SLRI, and (b) the corresponding porosity evolution (compaction of the water ice–rock mixture is computed after Leliwa-Kopystynski and Kossacki, 1995). (c) Thermal model for $t_{0\text{-CAIs}} = 2.5$ Myr; (d) Thermal model for $t_{0\text{-CAIs}} = 5$ Myr. In all of these three cases, $h_a = 0.5$ and the initial concentration of $^{60}Fe/^{56}Fe$ is 0.5×10^{-6}.

ence in the effects between small versus large icy satellites. In the latter, it is expected that accretional heat will produce partial to full melting of the volatile component. In our models, to treat the effects of ammonia we assume that ammonia is present is sufficient quantity to trigger early differentiation.

The major effect of including ammonia is that porosity decreases at a significantly lower temperature, ∼100 K, and this temperature is reached early in Iapetus' history. As a result the body effectively eliminates porosity almost from the start. Depending on the time of formation with respect to CAIs, melting of the interior occurs between a few Myr and 1 byr after formation (for the no SLRI case). In that case (Fig. 8a) only the inner region reaches the ammonia–water eutectic while the outer 400 km remains at lower temperatures. Indeed, if ammonia results in a decrease in thermal conductivity (by a factor 1.5; Lorenz and Shandera, 2001), the outer shell is less insulating than when it had 25 to 40% porosity. This means that the model gets colder than the one described in Section 4.2. In a few hundred Myr the water–ammonia ocean freezes. The 150-km radius core is too small to trigger any significant low viscosity, hot upwelling in which tidal dissipation could become significant (as has been described for Europa, e.g., Sotin et al., 2002).

If SLRI accreted in the satellite, then full melting of the interior can be complete a few Myr after formation. A rocky core up to 350 km in radius (Fig. 8b) can form. It is possible that some serpentinization of the rock occurs as a result of hydrothermal circulation at the surface of the core but the details of such processes are beyond the scope of this paper. The ocean is frozen by about 100 Myr after formation. The conditions need to be further studied for the case in which the core triggers heating-from-the-bottom type of convection which, in turn, develops hot plumes that go upward through the ice shell effectively all the way up to the surface (e.g., Deschamps and Sotin, 2001).

At the interface between the icy shell and the rocky core an ammonia-rich layer can have a viscosity as low as 10^{14} Pa s at temperatures close to the ammonia–water melting point, as has been experimentally measured by Arakawa and Maeno (1994). Depending on the amount of ammonia accreted in the satellite, this ammonia–hydrates layer can have a thickness of a few km (if 1 wt% NH_3 with respect to the total volatile amount) to several tens of kilometers (if >5 wt% NH_3). As such, it could represent a significant volume in which tidal dissipation, leading to despinning, would take place. However, experiments such as the ones carried out by Arakawa and Maeno (1994) are scarce and, thus, the lack of data prevents the meaningful modeling of such a scenario.

In summary, the addition of ammonia in models with LLRI only yields models too cold to match Iapetus' current state. Ammonia alone is not sufficient to produce successful models. The addition of SLRI may create conditions for despinning, but they are not modeled in detail.

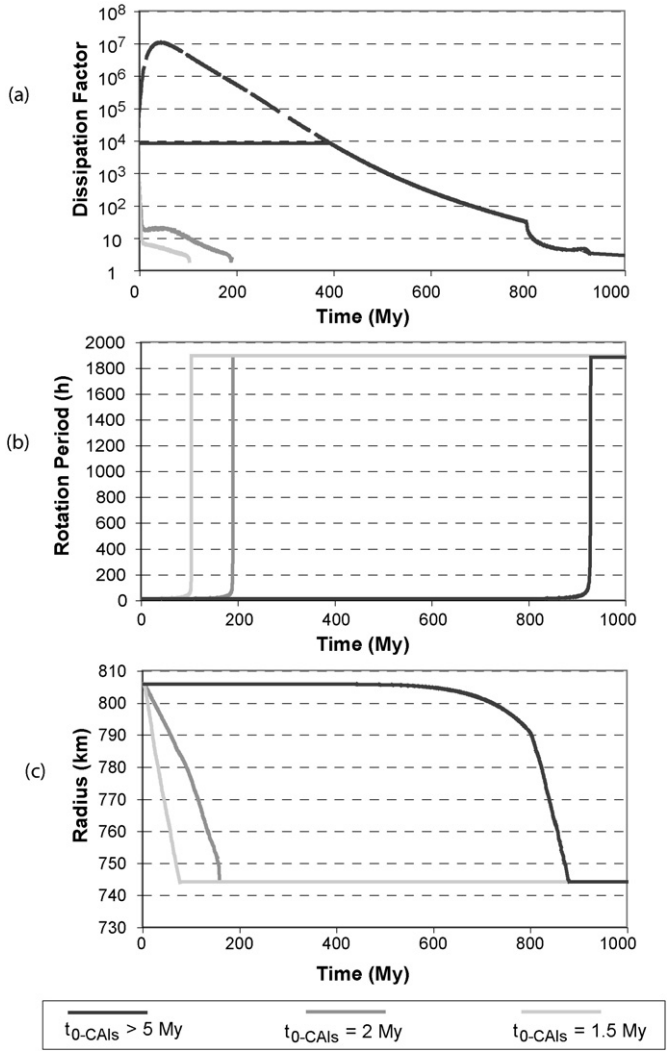

Fig. 9. Evolution of parameters versus time for different models that include SLRI. The ordinates are (a) the dissipation factor Q, (b) the rotation period in hours, (c) the equatorial radius in km. The time scale on the abscisses is linear. There is no significant change after 1 byr. The dissipation factor is fixed to 10^4 when the Maxwell body predicts greater values for this parameter (dashed curve).

4.5. Model summary

We have described models of Iapetus that despin in a reasonable time compared to the age of the Solar System. A subset of these models become stiff enough so that they preserve the 16-h shape until present. Successful models include SLRI in the accretion of Iapetus. Two major properties distinguish models with and without SLRI. First, SLRI play a "strategic" role by decreasing porosity early in the history. As a result in the long-run the lithosphere should be stronger than in the models without SLRI. Second, porosity plays a significant role in insulating the interior and reducing heat loss. Interestingly, models with SLRI and no porosity can get colder than porous models without SLRI.

In our models despinning is a highly non-linear process since the despinning rate is a function of the volume of material conducive to dissipation. This is accomplished by decreasing Q and increasing k_2 both of which are a function of time and temperature. For most of the models, despinning is negligible for most of their history. However, when the dissipative properties reach the critical values, the despinning process itself takes only a few millions years.

In the next section, we discuss the conditions for explaining some of Iapetus' major characteristics, i.e., the non-hydrostatic equatorial bulge and the equatorial ridge.

5. Discussion

We have found models that successfully explain Iapetus' present spin rate and shape. These models include SLRI, whose initial amount is a function of the constraints imposed by observations. This has consequences for dating the time of formation of Iapetus with respect to the creation of CAIs. This result implies that the satellite formed in less than 5 Myr after CAIs were formed.

In this section we consider whether it is possible to refine the determination of the time of formation of Iapetus with respect to CAIs. First we discuss the influence on the results of the assumptions on the modeling (Section 5.1). In the remainder of the discussion we address the implications of these results.

5.1. Modeling constraints and assumptions

5.1.1. One-dimensional modeling

In our models we have considered the situation at the equator. However in the early part of the evolution, the model bodies are highly oblate. The primary consequence of this is for heat transfer. This is especially true just after formation, when the rotation period is small and there is a ratio of at least 1.5 between the equatorial radius and the polar radius (Fig. 4). This also produces latitudinal variations of insolation, thus in the surface temperatures. This means that the timings given for the evolution of porosity will have some variation with latitude. Other consequences, for example, on surface relaxation, are addressed in Section 5.3. Compared to our models, an early, oblate Iapetus would lose somewhat more heat than we calculate. This affects the calculation of the amount of initial heat that comes from accretion and SLRI. Since the dependence of accretion date on heat is steep, these effects move the solutions only slightly toward earlier times. Since our range is relatively large ($2.5 < t_{0\text{-CAIs}} < 5.0$ Myr) we have not refined the precision further for the present paper.

5.1.2. Convection

There are two periods during which convection might start: (a) in the early history (<10 Myr after formation), as a result of the sudden heat production due to SLRI decay; (b) later, while LLRI decay progressively warms up the deep interior (e.g., the central 400 km) at temperature larger than 240 K in the successful case displayed in Fig. 7. Discussing the likelihood of convection is important because convection may stop the temperature increase required to get a viscosity low enough for despinning. As mentioned earlier, our main model assumption is that early convection, before despinning, did not occur.

In models such as the one illustrated in Fig. 7, the onset of convection derived from laboratory experiments and numerical work occurs when convective instabilities start as the viscosity becomes lower than 10^{15} Pa s (Sotin et al., 2006). With the viscosity law used in the present study, this viscosity translates into a temperature larger than 240 K. This temperature is reached before despinning for radii less than about 400 km. In 3-D Cartesian coordinates convection of a volumetrically heated fluid is driven by fast, cold downwelling plumes and slow upwelling of the relatively hot bulk material (Parmentier et al., 1994). There has been very little work in 3-D spherical geometry to date. For example, the work by Vangelov and Jarvis (1994) considered Rayleigh–Benard convection in a spherical shell. There are two main issues that may stop the downwelling plumes from moving down to the center of the satellite. First, for a given solid angle, the spherical geometry for such a small sphere implies surface shrinking that would very quickly limit the relative amount of hot bulk material compared to the amount of cold plume material. Second, gravity decreases toward zero as the center is approached. For radii between 400 and 200 km, the gravitational acceleration decreases by a factor of 2, resulting in a severe decrease in the buoyant force. These two effects may constrain any convection to a shell between about 200 and 400 km from the center, leaving the center of the satellite free of convection. It must be noted that in order for despinning to proceed, it is necessary to have a core of about 200 km at a low viscosity (high temperature).

If the accretion time is short (Fig. 12a), then temperatures larger than 240 K are attained at shallow depths. A recent study (Sotin et al., 2006) has shown that the onset of convection in a volumetrically-heated fluid cooled from above can be estimated using the predictions for a hot fluid as described by Korenaga and Jordan (2003). Convection starts once the internal viscosity, which is strongly temperature-dependent, reaches the critical value for the cold-fluid-above to become unstable. The scaling rules that govern the onset of convection have been studied in the case of a hot fluid cooled from above (Davaille and Jaupart, 1994; Choblet and Sotin, 2000; Korenaga and Jordan, 2003; Solomatov and Barr, 2006; Zaranek and Parmentier, 2004). We have conducted several numerical runs that have investigated this question in Cartesian coordinates with a viscosity that is only temperature-dependent. The temperature-dependence of viscosity is critical to initiating the onset of convection. As the fluid cools from above, a relatively dense cold layer builds up but its viscosity is too large for convective instabilities to start immediately. A conductive lid forms. At its base is located a thermal boundary layer where instabilities can grow. The convective instability begins once the thickness of the thermal boundary layer and its Rayleigh number reach critical values and the viscosity contrast across the thermal boundary layer is less than one order of magnitude (Solomatov and Barr, 2006). These rules have been applied to convective instabilities in large icy satellites (Barr et al., 2004), instabilities of the oceanic lithosphere (Korenaga and Jordan, 2003) and the onset of convection for Mars (Choblet and Sotin, 2000). Although these models can be applied to instabilities at shallow depth, they are designed to describe what happens much deeper in the satellite where curvature and gravity variations must be taken into account.

There are at least two additional complexities that need to be discussed. First, the viscosity used for convection is not the same as that used for tidal dissipation, which is frequency-dependent. At temperatures above 240 K, the dissipation factor varies by a factor of 2 to 10 between different models. As a result the situation can be favorable to both despinning and convection. In such a case, because despinning is a very rapid process with respect to the time needed for convection to set in, despinning will be complete before convection reaches steady-state.

Second, the onset of convection is further delayed by the accretional temperature profile, which is coldest at the center and warmest near the surface. This is not conducive to convection and must be overcome before convection can start. According to our modeling this takes 10 to 300 Myr.

Application to models

(a) Early history: Depending on the temperature at which convection starts, it takes from 2 Myr (at 250 K) to 20–200 Myr (at 220 K) to reach steady-state (Sotin et al., 2006). However, the heat pulse due to SLRI decay lasts less than 10 Myr and cannot sustain the development of convection. Numerical simulations suggest that convection would exist for a few million years. As soon as convection starts, the amount of heat that can be removed exceeds radiogenic heating. Convection cools the interior down to a temperature at which viscosity becomes too high for convection to continue. With the viscosity law used in the present study, convection stops when the temperature is equal to 220 K. Then, the LLRI are the only heat source. The heating rate is such that high temperature can be attained only at large depths. It is then possible that convection may have existed very early in Iapetus history, preventing high temperature (i.e., low viscosity) from being achieved and not permitting despinning during these first several millions of years.

(b) Late history: In the late stage, the time needed for LLRI to heat the deep interior up to 240 K (the temperature for the onset of convection), can be several hundred Myr years. The arguments developed above on the effect of sphericity and the lack of numerical work on convection in an infinite Prandtl number, volumetrically heated, self-graving sphere, lead us to assume that an inner core about 200 km in radius could be left free of convection and provide the low viscosity volume where tidal dissipation leads to despinning.

This information can be used to constrain the amount of SLRI needed in Iapetus, as discussed in Section 5.7.

5.2. Context for forming the ridge

From Iapetus' thermal evolution models we have identified two periods when significant changes in surface area occur: when porosity decreases as a result of internal warming, and when oblateness evolves as a result of despinning. These mod-

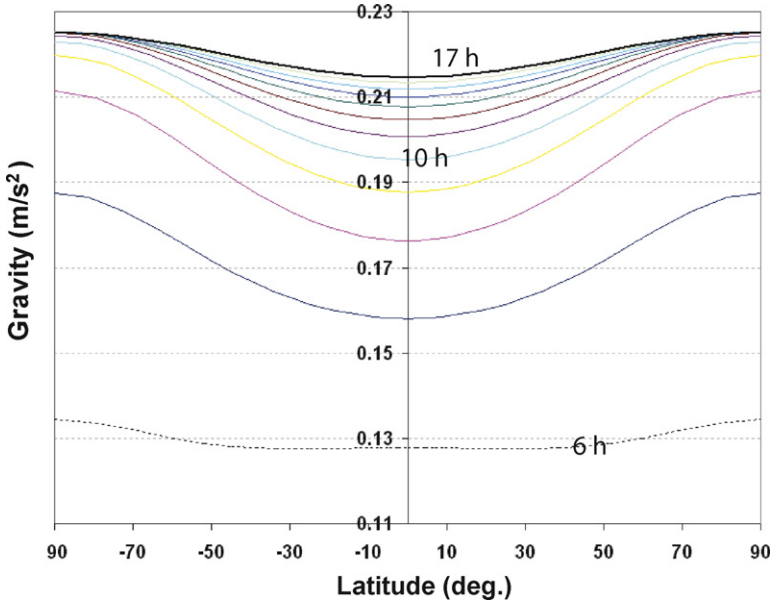

Fig. 10. Surface gravity as a function of latitude, and as a function of rotation rate (in hours) while Iapetus despins toward synchronous rotation. The initial rotation period assumed in our models is 7 h. The Roche's limit is 3.8 h.

els also provide the evolution of the lithospheric thickness. Because despinning is highly non-linear, the changes in radius and associated surface area reduction (thus the strain rate applied to the lithosphere) also vary non-linearly with time. Times when large decreases in surface area occur are optimum times for tectonic activity. The amount of material available to be redistributed is a function of the initial rotation period. If we take an initial rotation period of 5 h, the net change in surface area while despinning to 16 h is -0.23×10^6 km^2. Using the thin shell approximation and taking the lithosphere as 15 km thick, the volume of material theoretically available for redistribution would be $\sim 3.5 \times 10^6$ km^3. This compares well with the volume of the ridge of $\sim 3 \times 10^6$ km^3 estimated in Section 2.3. Thus, the change in surface area associated with despinning can yield the correct order of magnitude for the volume of material needed for ridge building. The greatest uncertainty in the above calculation is likely to be that the lithospheric value should have been thicker, yielding more volume. However, this is only one possibility.

Another source of volume change and stress development is compaction. Decreasing porosity builds stress in the lithosphere and enhances the conditions for tectonic activity while the lithosphere is very thin. While this remains to be modeled in two dimensions, we anticipate that compaction starts at the equator, then spreads to progressively higher latitudes until the poles are reached. This is governed by the subsurface temperatures.

In all models including SLRI, the lithosphere becomes thinner than 20 km within 10 Myr following accretion. This period is also accompanied by compaction of the material. When despinning occurs, later, the lithosphere is much thicker.

The formation of the ridge at the equator might occur at this stage because this is the locus and time of the maximum area change and hence the largest volume of material available for ridge construction. This location is also favored from an energy point of view: it was easiest to lift mass at the equator due to the reduction of gravity by the maximum available centrifugal force (Fig. 10). Here, the restraining forces on the upward buckling of the plate were minimal.

At this stage, it is not possible to conclude how and when the ridge formed. Either it was within the first 10 Myr after accretion when the lithosphere was of the order of 15 km thick, or later as a result of the decrease in radius resulting from despinning.

5.3. Why a "16-h shape"?

The fossil 16-h shape marks a critical crossing point of the dynamical model and the thermo-physical model for the evolution of the interior. As Iapetus despins, its hydrostatic figure becomes more spherical. We have calculated that the mechanical lithosphere must be at least 230 km thick when the rotation period reaches ~16 h, assuming the lithosphere is made of pure, solid water ice. This conjunction of processes depends upon the cooling of the lithosphere, whose thickness increases with time. Thus, at the first moment when its stiffness becomes sufficient to resist the relaxation of the global hydrostatic figure, continuous relaxation ceases and the shape becomes "frozen." As mentioned earlier, we have used a static criterion, based on the intrinsic strength of the satellite, without modeling the potential effect played by relaxation.

The relaxation as a function of time is given by (e.g., Turcotte and Schubert, 2002)

$$w = w_{\mathrm{m}} e^{-t/\tau}, \tag{4}$$

where τ is the characteristic relaxation time given by

$$\tau = \frac{4\pi\eta}{\rho g \lambda}, \tag{5}$$

where λ is the wavelength.

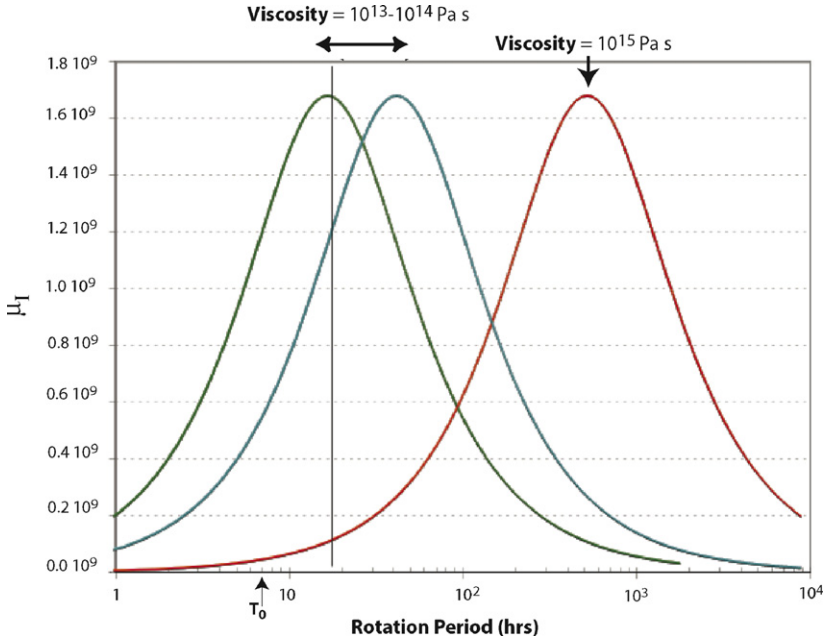

Fig. 11. Tidal dissipation factor versus rotation period for three different ice viscosities. The ordinate, μ_I, is the imaginary part of the shear modulus. The curves are for global dissipation in a homogeneous satellite. The first two curves from the left bracket water ice at its melting point. The curve on the right shows the dissipation for a temperature 5 K below the melting point. T_0 is the 7-h period with which the models were started.

Because of the long wavelength of the shape of the non-hydrostatic deviation, the viscosity has to be at least 10^{20} Pa s for relaxation to operate on time scales longer than several tens of millions of years. The problem is obviously more complicated as relaxation is a function of the viscosity gradient, as described by Nimmo (2004b).

All of the models in this paper employ Maxwell rheology. In a Maxwell body dissipation is strongly dependent on rotation frequency for a given viscosity. Fig. 11 shows the evolution of the shear modulus imaginary component, which is proportional to tidal dissipation shown for three viscosities. In our calculation both rotation rate and viscosity change with time. The path followed by the dissipation factor during Iapetus' thermal evolution is shown in Fig. 9 for several cases. At temperatures greater than 240 K the Maxwell rheology is a good approximation for modeling the material behavior (Tobie et al., 2005).

For rotation periods between 10 and 100 h, the viscosities at which maximum dissipation is achieved are less than 10^{15} Pa s. For greater viscosities, the time scale for despinning from the initial rotation period of less than 10 h, to the periods that are optimum for dissipation is much longer than the time scale for warming the satellite as a result of LLRI decay and reducing its viscosity. As a result the viscosity reaches values between 10^{13} and 10^{15} Pa s, which is ideal for dissipation while the rotation period is between 13 and 17 h.

The fact that despinning is such a sudden process is key to maintaining a frozen shape, since the relaxation of the shape would take several hundred Myr. During this period the body freezes.

5.4. Comparison with other satellites

Why are there not other satellites like Iapetus? The processes we have used in explaining Iapetus are perfectly general and should be applicable everywhere. The answer lies in the nonlinearity of these processes. Consider Rhea, which is about Iapetus' size. Rhea differs from Iapetus by: (1) its distance to Saturn that significantly reduces the time needed for despinning it to its present synchronous rotation period of 4.51750 days (Eq. (1)), and (2) its rock mass fraction that is 50% greater than that of Iapetus' (Thomas et al., 2007). If we use Rhea's parameters in our models, we find that the despinning takes $\sim 10^4$ yr. Thus, it took place during the heating by SLRI decay at a time when the lithosphere would have been too thin (<5 km) to support any significant non-hydrostatic loads such as Iapetus' shape. In fact Rhea's shape is within a few km from its hydrostatic shape for its current spin rate. Also, if a ridge formed in association with despinning, it should have relaxed and there would be nothing to be seen today.

Iapetus is indeed a special case due to its unique location on the edge of the regular saturnian satellite system. Other satellites are either too close to Saturn or have a larger rock fraction, or both.

5.5. Origin of Iapetus

It has been previously concluded that despite its distance to Saturn, Iapetus' origin is compatible with that of a regular satellite (Ward, 1981). Further evidence can be inferred from its composition, which, compared to Phoebe, indicates an enrichment in volatiles and organics (Johnson and Lunine, 2005). We can now add geodetic and geological evidence to further support this conclusion. The despinning of Iapetus can only take place in the presence of a massive primary object. This despinning history, together with thermophysical evolution, is required to explain the non-hydrostatic shape and the equatorial ridge. These can only occur as they did at approximately

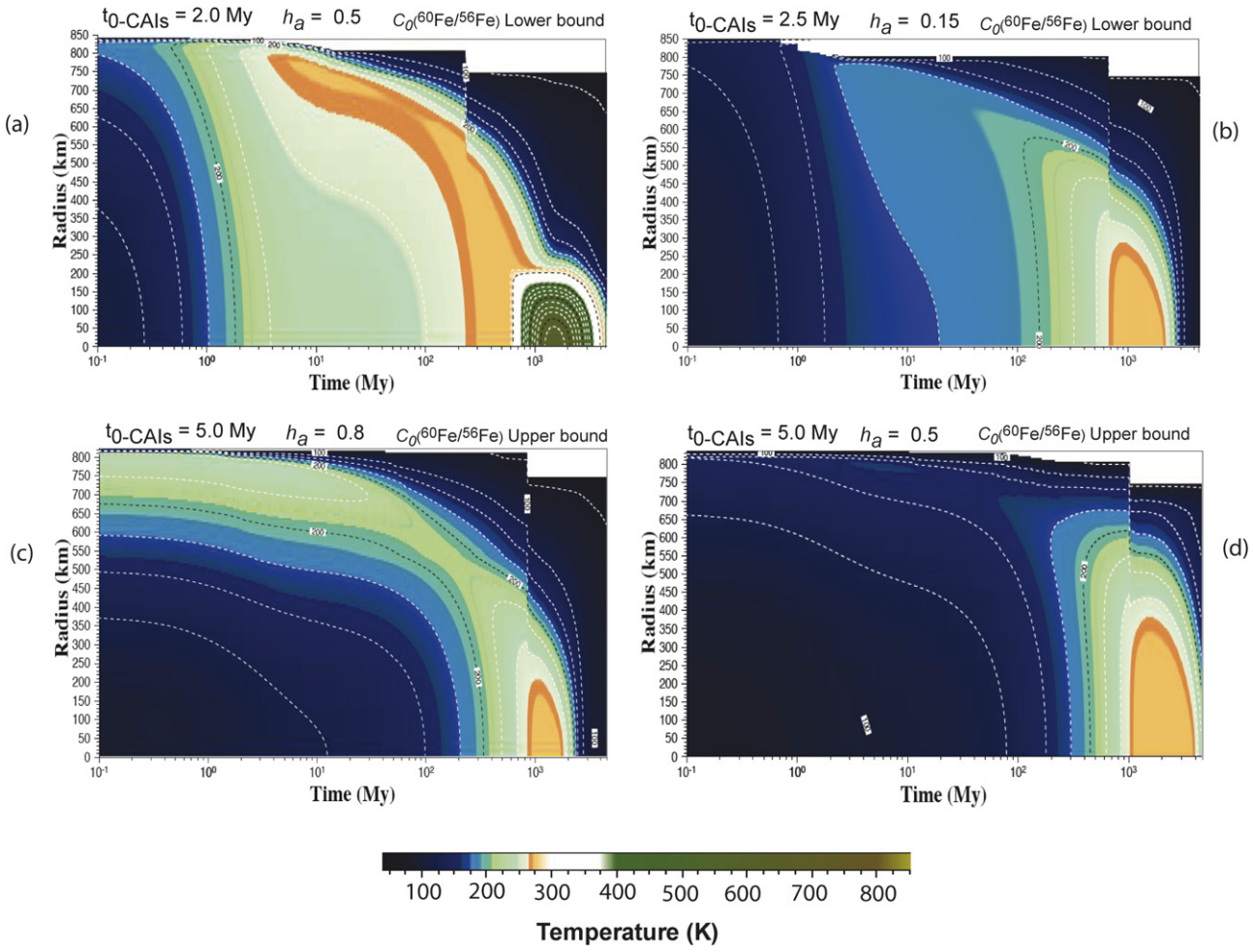

Fig. 12. Same models as shown in Fig. 7 but for some different times of formation with respect to CAIs, $t_{0\text{-CAIs}}$, different initial concentrations in ^{60}Fe, and different values of the accretional parameter h_a. See Section 5.7 for discussion.

Iapetus' position in the gravity field of a large planet like Saturn.

5.6. Implications for cratering and age

Iapetus' surface is the most heavily cratered among the surfaces of the saturnian satellites (Porco et al., 2005) and presumably has a crater age relatively close to its time of accretion.

From thermal evolution modeling (e.g., Fig. 7) it is possible to infer constraints on the time at which the lithosphere was able to record craters. We apply Appendix C.1 equations to determine that the lithosphere was able to record craters a few tens of millions of years after the satellite's formation, and the large basins about 100 Myr after formation.

Despinning took place between 200 and 900 Myr after formation, which opens the door to constraining the time of despinning vs the end of late heavy bombardment (which took place between 600 and 800 Myr after formation) if it occurred at Saturn. Indeed, the fact that a large, old, non-hydrostatic topographic anomaly was not seriously affected by cratering holds clues about the characteristics and impact chronology in the saturnian system.

Also, a direct result of our models is that the lithosphere did not undergo any endogenic activity (such as volcanism) later than 200 Myr after formation. As mentioned in Section 3.2.2.2, little orbital evolution and tidal dissipation took place that could have played a significant role in the geophysical evolution of the satellite after it became synchronous.

Thus Iapetus' surface may be the oldest in the Solar System, as close to an initial post-accretionary surface as we are likely to see.

5.7. Absolute chronometry

Our successful models include SLRI. For these models we find that the thermal evolution is effectively determined by the heat from accretion and SLRI decay. We use this constraint on the amount of SLRI to set the time of Iapetus' accretion relative to the time of formation of CAIs.

While the initial porosity is not well constrained, it does not play a significant role in the long-term evolution because the collapse of porosity throughout the model occurs within a few Myr after accretion. Thus, the main, variable parameters are h_a, $t_{0\text{-CAIs}}$, and the initial concentration of ^{60}Fe. We have performed a parametric study to test the effect of these three parameters.

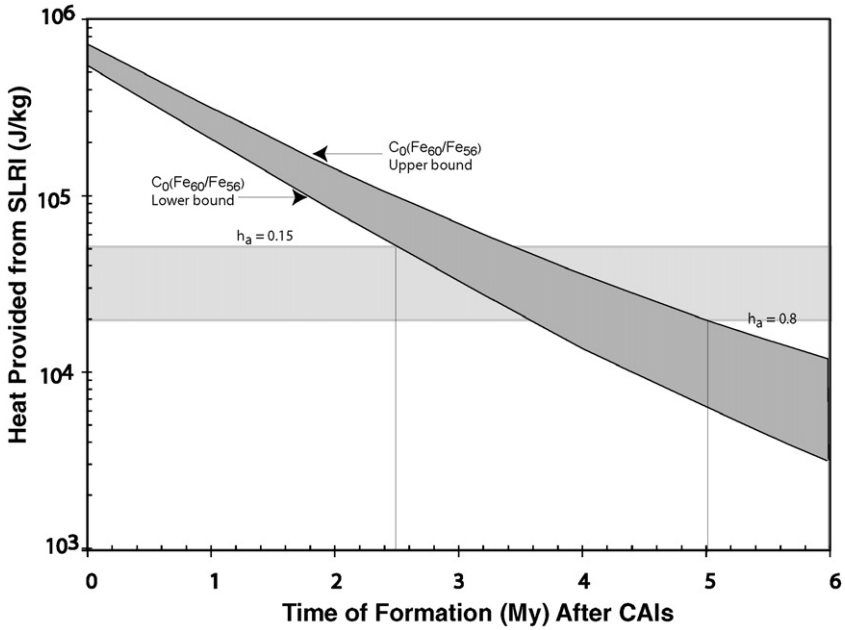

Fig. 13. Link between the heat needed for Iapetus' thermal budget and its formation time with respect to CAIs. The dark grey zone corresponds to the heat produced by SLRI allowing for the uncertainties in the composition and initial isotopic ratios. The width of this zone is chiefly due to the uncertainty in the initial abundance of ^{60}Fe. The light grey zone indicates the amount of heat that must be provided for Iapetus to despin and yet preserve its non-hydrostatic shape until present. The upper bound assumes little heat is provided by accretion and thus more is needed from SLRI. The lower bound is set by $h_a = 0.8$, and less heat is needed from SLRI. The intercept between the two zones yields the time of formation of Iapetus with respect to CAIs. Uncertainties in all the other modeling parameters are relatively small and, we believe, that they are covered by the width of the light grey band shown in this plot.

We considered an order of magnitude uncertainty in the initial concentration of ^{60}Fe; we took $h_a = 0$ to 1; we varied $t_{0\text{-CAIs}}$ between 1 and 7 Myr. Endmember results are discussed below and displayed in Fig. 12.

The early decrease of porosity is the combined result of accretional and SLRI heating. In the few Myr following accretion, temperature must reach values high enough for porosity to decrease, while avoiding the development of a warm interior in the long term. As a result, we do not find any successful models if h_a is less than 0.15.

For SLRI to play a role in Iapetus' despinning, it is necessary for $t_{0\text{-CAIs}}$ to be less than 5.0 Myr (Figs. 12c and 12d). However, for the shape to be preserved, the satellite cannot form before 1.5 Myr after CAIs, otherwise despinning occurs within a few Myr after formation while the body is still very warm and the lithosphere is thin (Fig. 12a). For $t_{0\text{-CAIs}}$ less than 2.5 Myr, convection starts and effectively stops the despinning before synchronous rotation can be achieved. For times between 1.5 and 2.5 Myr, successful models may exist, as we stated in Section 5.1.2. In the range $2.5 < t_{0\text{-CAIs}} < 5.0$ Myr convection does not play a significant role. Thus, between these dates we have an infinite set of successful models (e.g., Fig. 12b).

Since the amount of heat needed for our successful models is available only over a relatively small range of the SLRI decay curve, this requirement ties the Iapetus models to the "^{26}Al-decay chronology." This chronology is also a function of the initial abundance of ^{60}Fe, for which there is no consensual, "canonical" value in the literature, as this is an area of current research. We have used a large range, which includes the concentration values published over the last four years (see Chen et al., 2007 for a review).

While different studies conclude that ^{60}Fe must be produced from supernova injection, there are two contending models for the origin of ^{26}Al: the X-Wind model (Shu et al., 1996), which was formulated to match the available ^{26}Al data from inner Solar System objects (e.g., meteorites), and the supernova injection model (Vanhala and Boss, 2002). Simulations of this model by Boss (2006) indicate that the distribution of ^{26}Al and ^{60}Fe should be quasi-homogeneous in the Solar System. If the initial concentrations measured for ^{26}Al/^{27}Al and ^{60}Fe/^{56}Fe are homogeneous throughout the Solar System, it is possible to constrain the time of formation of Iapetus with respect to the formation of CAIs (Fig. 13). Analysis of the parameter space yields bounds on Iapetus' time of formation between 2.5 and 5.0 Myr after CAIs. If we accept the Pb–Pb age of CAIs measured by Amelin et al. (2002) of 4567.2 ± 0.6 Myr, then the age of Iapetus is between 4562.2 and 4564.7 Myr. Systematic uncertainties in this estimate include the actual distribution of ^{26}Al and ^{60}Fe in the solar nebula.

Since Iapetus is almost certainly a regular satellite of Saturn, rather than a captured object (Canup and Ward, 2006), the absolute chronology obtained sets a limit of five million years for the formation of Saturn after the appearance of CAIs. This is consistent with the independent evidence that the time scale for giant planet formation is millions, rather than tens of millions, of years. Recent astronomical observations suggest that the lifetime around Sun-like stars of sufficient gas to make giant planets may be typically only two to five million years (Najita and Williams, 2005). Models for the formation of giant planets

by direct collapse can easily meet this time constraint (Mayer et al., 2002). The nucleated instability model of giant planet formation may be more relevant to the giant planets of our own Solar System, with their supersolar heavy element abundances and regular satellite systems, but only under certain restricted conditions do they seem able to produce gas giant planets within a few million years (Lissauer and Stevenson, 2007).

A somewhat weaker constraint on giant planet formation time scales comes from dynamical calculations that show the presence of Jupiter and Saturn to be important determinants of the final architecture of the terrestrial planet orbits and masses (O'Brien et al., 2006), coupled with the fact that much of the growth of the Earth was completed within 10–30 million years after CAIs based on the Hf–W isotopic system. Our time scale result provides an additional indication that giant planet formation was relatively rapid in our own Solar System and gives impetus to the further development and elaboration of the nucleated instability models for giant planet growth.

The precision of the Iapetus modeling result will help support a better understanding of the links between the different chronological scales such as those derived from nucleosynthesis, formation of the first solids, meteorites, crater counting, and radiometric dating.

6. Conclusions

We have modeled the geophysical history of Iapetus based upon discoveries from the *Cassini–Huygens* mission, modeling of several interconnected physical processes, and updated properties for materials and the processes that operate upon them. We have considered a range of different initial assumptions, i.e., the initial porosity distribution in the satellite, initial temperature profile at the end of accretion, the presence or absence of SLRI, the presence or absence of significant amounts of ammonia, and the date of accretion with respect to CAIs.

We show that despinning is a non-linear process, and that it has significant effects on Iapetus' geology. Depending upon the initial conditions, synchronous rotation is achieved between 200 Myr and 1 Byr after formation. At the time of despinning the lithosphere must have become strong enough to preserve the non-hydrostatic figure seen today. It is important to note the key role played by SLRI in decreasing the porosity early in Iapetus' history. This allows heat to escape faster and leads to the development over the long run of a thick, mechanically strong, lithosphere, suitable, just in time, for preserving the 16-h figure.

We found that there were two large reductions in surface area that took place in Iapetus' history. The first was due to a decrease in porosity and the second was due to despinning. We note the potential geological role of either or both of these two events in the formation Iapetus' equatorial ridge.

Models without SLRI do not work no matter what the ammonia concentration. With SLRI we have a range of models that work, although such models including ammonia require more study.

Another general result is that in all of the models where convection may be an issue, the onset of convection in the outer layer acts to frustrate early despinning. Since Iapetus demonstrably did despin to synchronous rotation, we conclude that convection, if it occurred, did not prevent the formation of a low-viscosity core.

Given the scope and importance of the conclusions that have come out of this study, further modeling and investigation is definitely warranted. We have taken care throughout the paper to point out the various uncertainties, limits on our knowledge, and paths not pursued. All of these are worthy topics for future research.

The notion that a high precision, absolute chronology of the outer Solar System can be obtained through the properties of the natural satellites is truly novel.

Acknowledgments

We thank B. Bills and an anonymous reviewer for their comments and suggestions. We are also very grateful to F. Nimmo whose careful review helped significantly enhance the quality of this manuscript. We thank G. Schubert, W. Moore, and D. Stevenson for many discussions. We thank E. Turtle and T. Denk for discussions of the geology of Iapetus. J.C.C.-R. and D.L.M. thank T. Spohn, W. Ward, R. Canup, G. Huss, S. Krot, R. Pappalardo, and G. Tobie for useful discussions. C. Sotin was a Distinguished Visiting Scientist at JPL during the course of this effort. J. Lunine was a Distinguished Visiting Scientist at JPL and a Visiting Professor at Istituto di Fisica dello Spazio Interplanetario, INAF, Rome, Italy, during the course of this effort. This work was carried out at the Jet Propulsion Laboratory, California Institute of Technology under a contract from NASA. We acknowledge support from the NASA Planetary Geology and Geophysics Program. This work was done while J.C.C.-R. was a postdoctoral scholar at the California Institute of Technology.

Appendix A. Thermal evolution

This appendix refers to Section 3.2.1 in the text.

A.1. Conduction equation

Heat is transferred by conduction using

$$\frac{\partial(k(T)\partial T(r)/\mathrm{d}r)}{\partial r} + \frac{2}{r}\left(k(T)\frac{\partial T(r)}{\partial r}\right) = \rho(r)C_{\mathrm{p}}(T)\left(\frac{\mathrm{d}T(r)}{\mathrm{d}t}\right) - H(r),$$

where T is temperature (in Kelvin), r local radius, k thermal conductivity, ρ material density, C_{p} specific heat, t time, H internal heating (e.g., radiogenic, tidal dissipation).

A.2. Accretional heat

Accretional heat is computed after Squyres et al. (1988). The temperature increase due to accretion is small. It can reach up to 90 K in the largest medium-sized satellites Rhea and Iapetus,

but represents only a few tens of degrees in the smallest satellites (Ellsworth and Schubert, 1983). Accretional temperature profile is computed from

$$T(r) = \frac{h_a}{C_p(T)}\left[\frac{4\pi}{3}\rho G r^2 + \frac{\langle v\rangle^2}{2}\right] + T_i,$$

where $\langle v\rangle^2$ is proportional to the Safronov parameter, h_a is the fraction of mechanical energy turned into heat, C_p is the temperature-dependent material specific heat. T_i is the temperature of the planetesimals at the time of accretion. The Safronov parameter ranges between 3 and 5 (Safronov, 1972). The value of h_a depends on the characteristics of the accretional processes, especially the accretion duration.

A.3. Gravitational energy

The shrinking (e.g., porosity collapse) and differentiation of the satellite result in converting potential gravitational energy into heat. This phenomenon has been studied and modeled by Leliwa-Kopystynscki and Kossacki (2000).

The specific gravitational energy of self-compaction (i.e., closing of pores is modeled using the equation from Leliwa-Kopystynscki and Kossacki (2000):

$$Eg = R_s^2\left[1 - (1-\Psi)^{1/3}\right] \times 0.8\pi G\bar{\rho} \text{ (in J/kg)}, \quad \text{(A.1)}$$

where $\bar{\rho}$ is the satellite's mean density, and Ψ is porosity.

A.4. Despinning heat

Despinning produces heat and is calculated using (Burns, 1976):

$$\Delta T = \frac{1}{2}\gamma\omega_0^2\frac{R_s^2}{C_p(T)},$$

where γ is the mean moment of inertia and ω_0 is the initial spin rate.

Appendix B. Tidal evolution

This appendix supports Section 3.2.2 in the text.

B.1. Despinning evolution

Spin rate evolution (ω, in rad/s) as a function of time, t, is given by

$$\frac{d\omega}{dt} = -\frac{3k_2(t)GM_p^2a^5(t)}{C(t)D^6Q(t)},$$

where G is the universal constant of gravity, M_p Saturn's mass, a Iapetus' equatorial radius, C the polar moment of inertia, and D the semi-major axis of the orbit. The dissipation factor Q and the tidal Love number k_2 are functions of the frequency-dependent viscoelastic properties of the satellite and thus vary as a function of time. The difficulty in despinning a distant satellite, such as Iapetus, results directly from the strong (inverse sixth power) dependence on D.

B.2. Eccentricity evolution

Eccentricity evolution is computed after Peale (1999). The time scale for eccentricity damping is a function of

$$e(t) = e_0\exp(\tau t),$$

where e_0 is the initial eccentricity, t is time and the damping time scale τ is defined by

$$\tau = \frac{57}{8}\frac{m_s}{m_p}\frac{R_p^5}{a^5}\frac{k_p}{Q_p}n - \frac{21}{2}\frac{m_p}{m_s}\frac{R_s^5}{a^5}\frac{k_s}{Q_s}n$$

with m_x mass, R_x radius, n Iapetus' mean orbital motion, e Iapetus' eccentricity at a given time, k_x dynamic potential Love number; Q_x dissipation factor; $x = $ s or p refers to Iapetus or Saturn, respectively. The first term expresses the effect on the planet and the resulting contribution that it makes to the time scale for eccentricity dampening. The second term is the contribution to the eccentricity damping time scale due to internal dissipation in Iapetus.

B.3. Love number and dissipation factor calculation

To obtain the *tidal Love* number and the *dissipation factor* directly we solve for values of the complex tidal Love number k_2, which is computed using a numerical integration of spheroidal eigenfunctions for a multilayered body (Takeushi and Saito, 1972; Castillo et al., 2000; Tobie et al., 2005). The dissipation factor is equal to $Q = -k_2/\Im(k_2)$ with $\Im(k_2)$ being the imaginary part of k_2.

For the Maxwell rheology, the shear modulus is a function of the excitation frequency, ω (i.e., mean orbital motion), the rigidity, μ, and the viscosity, η:

$$\mu_R = \frac{\eta^2\omega^2\mu}{\mu^2+\omega^2\eta^2}, \qquad \mu_I = \frac{\eta\omega\mu^2}{\mu^2+\omega^2\eta^2}.$$

The subscripts R and I indicate the real and imaginary parts, respectively.

Appendix C. Geological module

This appendix refers to Section 3.3 in the text.

C.1. Large non-hydrostatic anomaly preservation

The capacity of a lithosphere of thickness δ to retain topography can be described by how much it relaxes, w, under the topographic load h (Turcotte et al., 1981) of spherical harmonic degree n:

$$\frac{w_{nm}}{h_{nm}} = \left(\frac{\rho_c}{\rho_m-\rho_c}\right) \times\left[\frac{m-(1-\nu)}{\sigma(m^3-4m^2)+\tau(m-2)+m-(1-\nu)}\right]$$

with τ the spherical shell rigidity if bending resistance is neglected:

$$\tau = \frac{E\delta}{R^2g(\rho_m-\rho_c)}$$

and σ the bending rigidity

$$\sigma = \frac{\tau}{12(1-\nu^2)}\left(\frac{\delta}{R}\right)^2,$$

$m = n + 1$; E is Young's modulus; ν is Poisson's ratio.

The compensation degree C at the harmonic degree n is expressed as

$$C_n = \left(1 - \frac{3\rho_m}{(2n+1)\bar{\rho}}\right) \times \left[\frac{\sigma(m^3 - 4m^2) + \tau(m-2) + m - (1-\upsilon)}{m - (1-\nu)} - \frac{3\rho_m}{(2n+1)\bar{\rho}}\right]^{-1}.$$

For an icy interior such as Iapetus, the base of the mechanical lithosphere has been defined by Deschamps and Sotin (2001) as the temperature at which ice-creep is reached (e.g., 170 K).

C.2. Shape evolution due to despinning

The initial shape was discussed in Section 3.1.5. In this module we recompute the change in surface area that results from the change in shape with despinning. The surface area is given by

$$A = 2\pi a^2 + \pi(c^2/a^2)\ln\left[(1+\varepsilon)/(1-\varepsilon)\right],$$

where ε is the shape eccentricity:

$$\varepsilon = \left[1 - (c/a)^2\right]^{1/2}.$$

Notation: a equatorial axis, c polar axis.

References

Amelin, Y., Krot, A.N., Hutcheon, I.D., Ulyanov, A.A., 2002. Lead isotopic ages of chondrules and calcium–aluminum-rich inclusions. Science 297, 1678–1683.

Arakawa, M., Maeno, N., 1994. Effective viscosity of partially melted ice in the ammonia–water system. Geophys. Res. Lett. 21, 1515–1518.

Barr, A.C., Pappalardo, R.T., Zhong, S., 2004. Convective instability in ice I with non-Newtonian rheology: Application to the icy Galilean satellites. J. Geophys. Res. 109, doi:10.1029/2004JE002296. E12008.

Berryman, J.G., 1995. Mixture theories for rock properties. In: Ahrens, T.J. (Ed.), A Handbook of Physical Constants: Global Earth Physics. In: AGU Reference Shelf Series, vol. 1. ISBN 0-87590-851-9, pp. 205–228.

Boss, A.P., 2006. Isotopic heterogeneity associated with mixing and transport in the solar nebula. Lunar Planet. Sci. 37. Abstract 1066.

Buratti, B.J., Cruikshank, D.P., Brown, R.H., Clark, R.N., Bauer, J.M., Jaumann, R., McCord, T.B., Simonelli, D.P., Hibbitts, C.A., Hansen, G.B., Owen, T.C., Baines, K.H., Bellucci, G., Bibring, J.-P., Capaccioni, F., Cerroni, P., Coradini, A., Drossart, P., Formisano, V., Langevin, Y., Matson, D.L., Mennella, V., Nelson, R.M., Nicholson, P.D., Sicardy, B., Sotin, C., Roush, T.L., Soderlund, K., Muradyan, A., 2005. Cassini Visual and Infrared Mapping Spectrometer observations of Iapetus: Detection of CO_2. Astrophys. J. 622, L149–L152.

Burns, J., 1976. Consequences of the tidal slowing of Mercury. Icarus 23, 453–458.

Canup, R.M., Ward, W.M., 2006. A common mass scaling for satellite systems of gaseous planets. Nature 441, 834–839.

Castillo, J., Mocquet, A., Sotin, C., 2000. Detecting a deep ocean within Europa by means of geodetic measurements. C. R. Acad. Sci. Paris 330, 659–666.

Castillo, J.C., Matson, D.L., Sotin, C., Johnson, T.V., Lunine, J.I., Thomas, P.C., 2005. A geophysical study of Iapetus: The need for and consequences of ^{26}Al. Bull. Am. Astron. Soc. 37. Abstract 39.04.

Chandrasekhar, S., 1969. Ellipsoidal Figures of Equilibrium. The Silliman Foundation Lectures. Yale Univ. Press, New Haven.

Chen, J.H., Papanastassiou, D.A., Wasserburg, G.J., 2007. High-precision nickel isotopic analyses in meteorites. Lunar Planet. Sci. 38. Abstract 1753.

Choblet, G., Sotin, C., 2000. 3-D thermal convection with variable viscosity: Can transient cooling be described by a quasi-static scaling law? Phys. Earth Planet. Int. 119, 321–336.

Cole, D.M., 1995. A model for the anelastic straining of saline ice. Philos. Mag. A 72, 231–248.

Cole, D.M., 1998. Modeling the cyclic loading response of sea ice. Int. J. Solids Struct. 35, 4067–4075.

Davaille, A., Jaupart, C., 1994. Onset of thermal convection in fluids with temperature dependent viscosity: Application to the oceanic mantle. J. Geophys. Res. 99, 19853–19866.

De La Chapelle, S., Milsch, H., Castelnau, O., Duval, P., 1999. Compressive creep of ice containing a liquid intergranular phase: Rate-controlling processes in the dislocation creep regime. Geophys. Res. Lett. 26, 251–254.

Denk, T., Matz, K.-D., Roatsch, T., Wolf, U., Wagner, R.J., Neukum, G., Jaumann, R., 2000. Iapetus (1): Size, topography, surface structures, craters. Lunar Planet. Sci. 31. Abstract 1596.

Denk, T., Neukum, G., Helfenstein, P., Thomas, P.C., Turtle, E.P., McEwen, A.S., Roatsch, T., Veverka, J., Johnson, T.V., Perry, J.E., Owen, W.M., Wagner, R.J., Porco, C.C., and The Cassini ISS Team, 2005. The first six months of Iapetus observations by the Cassini ISS camera. Lunar Planet. Sci. 36. Abstract 2262.

Dermott, S.F., Murray, C.D., 1982. Asteroid rotation rates depend on diameter and type. Nature 296, 418–421.

Dermott, S.F., Malhotra, R., Murray, C.D., 1988. Dynamics of the uranian and saturnian satellite systems—A chaotic route to melting Miranda? Icarus 76, 295–334.

Deschamps, F., Sotin, C., 2001. Thermal convection in the outer shell of large icy satellites. J. Geophys. Res. 106, 5107–5121.

Durham, W.B., Kirby, S.H., Stern, L.A., Ragaini, K.A., 1989. Brittle and ductile behavior of ice/rock mixtures. Lunar Planet. Sci. 20, 254.

Durham, W.B., Kirby, S.H., Stern, L.A., 1998. Rheology of Planetary Ices in Solar System Ices. In: Astrophysics and Space Science Library (ASSL) Series, vol. 227. Kluwer Academic Publishers, Dordrecht, ISBN 0792349024, p. 63.

Durham, W.B., McKinnon, W.B., Stern, L.A., 2005. Cold compaction of water ice. Geophys. Res. Lett. 32, doi:10.1029/2005GL023484. L18202.

Ellsworth, K., Schubert, G., 1983. Saturn's icy satellites: Thermal and structural models. Icarus 54, 490–510.

Endal, A.S., 1980. Evolutionary variations of solar luminosity. In: Variations of the Solar Constant, NASA Conference Publication CP-2191, Goddard Space Flight Center, Maryland, November 5–7, pp. 175–181.

Garrick-Bethell, I., Wisdom, J., Zuber, M.T., 2006. Evidence for a past high-eccentricity lunar orbit. Science 313, 652–655.

Gavrilov, S.V., Zharkov, V.N., 1977. Love numbers of the giant planets. Icarus 32, 443–449.

Giese, B., Denk, T., Neukum, G., Porco, C.C., Roatsch, T., Wagner, R., 2005. The topography of Iapetus' leading side. Bull. Am. Astron. Soc. 37, 3.

Gounelle, M., Russell, S.S., 2005a. Spatial heterogeneity of short-lived isotopes in the solar accretion disk and early Solar System chronology. In: Krot, A.N., Scott, E.R.D., Reipurth, B. (Eds.), Chondrites and the Protoplanetary Disk. In: ASP Conference Series, vol. 341. Astronomical Society of the Pacific, San Francisco, p. 588.

Gounelle, M., Russell, S.S., 2005b. On early Solar System chronology: Implications of an heterogeneous spatial distribution of ^{26}Al and ^{53}Mn. Geochim. Cosmochim. Acta 69, 3129–3244.

Hillier, J., Squyres, S.W., 1991. Thermal stress tectonics on the satellites of Saturn and Uranus. J. Geophys. Res. 96, 15665–15674.

Jacobson, R.A., Antreasian, P.G., Bordi, J.J., Criddle, K.E., Ionasescu, R., Jones, J.B., Mackenzie, R.A., Meek, M.C., Parcher, D., Pelletier, F.J., Owen Jr., W.M., Roth, D.C., Roundhill, I.M., Stauch, J.R., 2006. The gravity field of the saturnian system from satellite observations and spacecraft tracking data. Astron. J. 132, 2520–2526.

Johnson, T.V., Lunine, J., 2005. Saturn satellite densities and the C/O chemistry of the solar nebula. Lunar Planet. Sci. 36. Abstract 1410.

Kita, N.T., Huss, G.R., Tachibana, S., Amelin, Y., Zinner, E., Nyquist, L.E., Hutcheon, I.D., 2004. Constraints on the origins of chondrules and CAIs from short-lived and long-lives radionuclides. In: Workshop on Chondrites and Planetary Disks. Abstract 9064.

Korenaga, J., Jordan, T.H., 2003. Onset of convection with temperature- and depth-dependent viscosity. Geophys. Res. Lett. 29, 29–32.

Kossacki, K.J., Leliwa-Kopystynski, J., 1993. Medium-sized icy satellites: Thermal and structural evolution during accretion. Planet. Space Sci. 41, 729–741.

Lambeck, K., Pullan, S., 1980. The lunar fossil bulge hypothesis revisited. Phys. Earth Planet. Int. 22, 29–35.

Langseth, M.G., Keihm, S., Peters, K., 1976. The revised lunar heat flow values. Proc. Lunar Sci. Conf. 7, 3143–3144.

Leliwa-Kopystynski, J., Kossacki, K.J., 1995. Kinetics of compaction of granular ices H_2O, CO_2 and $(NH_3)_x(H_2O)_{1-x}$ at pressures of 2–20 MPa and in temperatures of 100–270 K. Application to the physics of the icy satellites. Planet. Space Sci. 43, 851–861.

Leliwa-Kopystyński, J., Kossacki, K.J., 2000. Evolution of porosity in small icy bodies. Planet. Space Sci. 48, 727–745.

Lewis, J.S., 1971. Satellites of the outer planets: Their physical and chemical nature. Icarus 15, 174–185.

Lissauer, J.J., Safronov, V.S., 1991. The random component of planetary rotation. Icarus 93, 288–297.

Lissauer, J.J., Stevenson, D.J., 2007. Formation of giant planets. In: Reipurth, V.B., Jewitt, D., Keil, K. (Eds.), Protostars and Planets V. Univ. of Arizona Press, Tucson, pp. 591–606.

Lorenz, R.D., Shandera, S.E., 2001. Physical properties of ammonia-rich ice: Application to Titan. Geophys. Res. Lett. 28, 215–218.

Lunine, J.I., Stevenson, D.J., 1982. Formation of the Galilean satellites in a gaseous nebula. Icarus 52, 14–39.

Matson, D.L., Brown, R.H., 1989. Solid-state greenhouses and their implications for icy satellites. Icarus 77, 67–81.

Matsuyama, I., Mitrovica, J.X., Manga, M., Perron, J.T., Richards, M.A., 2006. Rotational stability of dynamic planets with elastic lithospheres. J. Geophys. Res. 111, doi:10.1029/2005JE002447. E02003.

Mayer, L., Quinn, T., Wadsley, J., Stadel, J., 2002. Formation of giant planets by fragmentation of protoplanetary disks. Science 298, 1756–1759.

McCarthy, C., Cooper, R.F., Kirby, S.H., Durham, W.B., 2006. Ice/hydrate eutectics: The implications of microstructure and rheology on a multiphase europan crust. Lunar Planet. Sci. 37. Abstract 2467.

McCord, T.B., Sotin, C., 2005. Ceres: Evolution and current state. J. Geophys. Res. 110, doi:10.1029/2004JE002244. E05009.

McKeegan, K.D., Aleon, J., Bradley, J., Brownlee, D., Busemann, H., Butterworth, A., Chaussidon, M., Fallon, S., Floss, C., Gilmour, J., Gounelle, M., Graham, G., Guan, Y., Heck, P.R., Hoppe, P., Hutcheon, I.D., Huth, J., Ishii, H., Ito, M., Jacobsen, S.B., Kearsley, A., Leshin, L.A., Liu, M.-C., Lyon, I., Marhas, K., Marty, B., Matrajt, G., Meibom, A., Messenger, S., Mostefaoui, S., Mukhopadhyay, S., Nakamura-Messenger, K., Nittler, L., Palma, R., Pepin, R.O., Papanastassiou, D.A., Robert, F., Schlutter, D., Snead, C.J., Stadermann, F.J., Stroud, R., Tsou, P., Westphal, A., Young, E.D., Ziegler, K., Zimmermann, L., Zinner, E., 2006. Isotopic compositions of cometary matter returned by Stardust. Science 314, 1724–1726.

McKinnon, W.B., 2002. On the initial thermal evolution of Kuiper Belt objects. In: Warmbein, B. (Ed.), Proceedings of Asteroids, Comets, Meteors—ACM 2002. International Conference, 29 July–2 August 2002, Berlin, Germany. ESA SP-500. ESA Publications Division, Noordwijk, Netherlands, ISBN 92-9092-810-7, pp. 29–38.

Mosqueira, I., Estrada, P.R., 2005. On the origin of the saturnian satellite system: Did Iapetus form in-situ? Lunar Planet. Sci. 36. Abstract 1951.

Mostefaoui, S., Lugmair, G.W., Hoppe, P., 2005. ^{60}Fe: A heat source for planetary differentiation from a nearby supernova explosion. Astrophys. J. 625, 271–277.

Mound, J.E., Mitrovica, J.X., Forte, A.M., 2003. The equilibrium form of a rotating Earth with an elastic shell. Geophys. J. Int. 152, 237–241.

Mousis, O., Gautier, D., Bockelée-Morvan, D., 2002. An evolutionary turbulent model of Saturn's subnebula: Implications for the origin of the atmosphere of Titan. Icarus 156, 162–175.

Najita, J., Williams, J.P., 2005. An 850 μm survey for dust around solar-mass stars. Astrophys. J. 635, 625–635.

Nimmo, F., 2004a. What is the Young's modulus of ice? In: Workshop on Europa's Icy Shell: Past, Present, and Future. Abstract 7005.

Nimmo, F., 2004b. Non-Newtonian topographic relaxation on Europa. Icarus 168, 205–208.

Nimmo, F., Pappalardo, R.T., Giese, B., 2003. On the origins of band topography, Europa. Icarus 166, 21–32.

O'Brien, D.P., Morbidelli, A., Levison, H.F., 2006. Terrestrial planet formation with strong dynamical friction. Icarus 184, 39–58.

Ostro, S.J., West, R.D., Janssen, M.A., Lorenz, R.D., Zebker, H.A., Black, G.J., Lunine, J.I., Wyec, L.C., Lopes, R.M., Wall, S.D., Elachi, C., Roth, L., Hensley, S., Kelleher, K., Hamilton, G.A., Gim, Y., Anderson, Y.Z., Boehmer, R.A., Johnson, W.T.K., and the Cassini RADAR Team, 2006. Cassini RADAR observations of Enceladus, Tethys, Dione, Rhea, Iapetus, Hyperion, and Phoebe. Icarus 183, 479–490.

Parmentier, E.M., Sotin, C., Travis, B.J., 1994. Turbulent 3D thermal convection in an infinite Prandtl number volumetrically heated fluid: Implications for mantle dynamics. Geophys. Int. J. 116, 241–259.

Peale, S.J., 1986. Orbital resonances, unusual configurations, and exotic rotation states among the planetary satellites. In: Burns, J.A., Matthews, M.S. (Eds.), Satellites. Univ. of Arizona Press, Tucson, AZ, pp. 159–224.

Peale, S.J., 1999. Origin and evolution of the natural satellites. Annu. Rev. Astron. Astrophys. 37, 533–602.

Peale, S.J., Cassen, P., Reynolds, R.T., 1980. Tidal dissipation, orbital evolution, and the nature of Saturn's inner satellites. Icarus 43, 65–72.

Porco, C.C., Baker, E., Barbara, J., Beurle, K., Brahic, A., Burns, J.A., Charnoz, S., Cooper, N., Dawson, D.D., Del Genio, A.D., Denk, T., Dones, L., Dyudina, U., Evans, M.W., Giese, B., Grazier, K., Helfenstein, P., Ingersoll, A.P., Jacobson, R.A., Johnson, T.V., McEwen, A., Murray, C.D., Neukum, G., Owen, W.M., Perry, J., Roatsch, T., Spitale, J., Squyres, S., Thomas, P.C., Tiscareno, M., Turtle, E., Vasavada, A.R., Veverka, J., Wagner, R., West, R., 2005. Cassini imaging science: Initial results on Phoebe and Iapetus. Science 307, 1237–1242.

Pravec, P., Harris, A.W., Michalowski, T., 2002. Asteroid rotations. In: Bottke, W.F., Paolicchi, P., Binzel, R.P., Cellino, A. (Eds.), Asteroids III. Univ. of Arizona Press, Tucson, AZ. 785 pp.

Prialnik, D., Bar-Nun, A., 1990. Heating and melting of small icy satellites by the decay of ^{26}Al. Astrophys. J. 355, 281–286.

Pritchard, M.E., Stevenson, D.J., 2000. Thermal aspect of a lunar origin by giant impact. In: Canup, R.M., Righter, K. (Eds.), Origin of the Earth and Moon. In: The University of Arizona Space Science Series. Univ. of Arizona Press, Tucson, pp. 179–189.

Reeh, N., Christensen, E.L., Mayer, C., Olesen, O.B., 2003. Tidal bending of glaciers: A linear viscoelastic approach. Ann. Glaciol. 37, 83–89.

Ross, R.G., Kargel, J.S., 1998. Thermal conductivity of Solar System ices, with special reference to martian polar caps. In: Solar System Ices. In: Astrophysics and Space Science Library (ASSL) Series, vol. 227. Kluwer Academic Publishers, Dordrecht, ISBN 0792349024.

Safronov, V.S., 1972. Accumulation of the Planets. In: Symposium on the Origin of the Solar System, held 3–7 April, 1972 in Nice, France. Edition du Centre National de la Recherche Scientific, Paris, p. 89.

Showman, A.P., Stevenson, D.J., Malhotra, R., 1997. Coupled orbital and thermal evolution of Ganymede. Icarus 129, 367–383.

Shu, F.H., Shang, H., Lee, T., 1996. Toward an astrophysical theory of chondrites. Science 271, 1545–1552.

Solomatov, V.S., Barr, A.C., 2006. Onset of convection in fluids with strong temperature-dependent, power-law viscosity. Phys. Earth Planet. Int. 155, 140–145.

Sotin, C., Head, J.W., Tobie, G., 2002. Europa: Tidal heating of upwelling thermal plumes and the origin of lenticulae and chaos melting. Geophys. Res. Lett. 29, 74–77.

Sotin, C., Castillo, J., Tobie, G., Matson, D.L., 2006. Onset of convection in mid-sized icy satellites. EGU, EGU06-A-08124.

Squyres, S.W., Reynolds, R.T., Summers, A.L., Shung, F., 1988. Accretional heating of the satellites of Saturn and Uranus. J. Geophys. Res. 93, 8779–8794.

Tachibana, S., Huss, G.R., 2003. The initial abundance of ^{60}Fe in the Solar System. Astrophys. J. 588, L41–L44.

Tachibana, S., Huss, G.R., Kita, N.T., Shimoda, G., Morishita, Y., 2006. ^{60}Fe in chondrites: Debris from a nearby supernova in the early Solar System? Astrophys. J. 639, L87–L90.

Takeushi, T., Saito, M., 1972. Seismic surface waves. In: Methods in Computational Physics, vol. 11. Academic Press, New York, p. 217.

Thomas, P.C., 1993. Gravity, tides, and topography on small satellites and asteroids: Application to surface features of the martian satellites. Icarus 105, 326–344.

Thomas, P.C., Parker, J.Wm., McFadden, L.A., Russell, C.T., Stern, S.A., Sykes, M.V., Young, E.F., 2005. Differentiation of the Asteroid Ceres as revealed by its shape. Nature 437, 224–226.

Thomas, P.C., Burns, J.A., Helfenstein, P., Squyres, S., Veverka, J., Porco, C., Turtle, E.P., McEwen, A., Denke, T., Giese, B., Roatsch, T., Johnson, T.V., Jacobson, R.A., 2007. Shapes of the saturnian icy satellites and their significance. Icarus, doi:10.1016/j.icarus.2007.03.012, in press.

Tobie, G., Mocquet, A., Sotin, C., 2005. Tidal dissipation within large icy satellites: Applications to Europa and Titan. Icarus 177, 534–549.

Turcotte, D.L., Schubert, G., 2002. Geodynamics, second ed. Cambridge Univ. Press, Cambridge, UK. 472 pp.

Turcotte, D.L., Willemann, R., Haxby, W.F., Norberry, J., 1981. Role of membrane stresses in the support of planetary topography. J. Geophys. Res. 886, 3951–3959.

Urey, H.C., 1955. The cosmic abundances of potassium, uranium and thorium and the heat balances of the Earth, the Moon, and Mars. Proc. Natl. Acad. Sci. USA 41, 127–144.

Vanhala, H.A.T., Boss, A.P., 2002. Injection of radioactivities into the forming Solar System. Astrophys. J. 575, 1144–1150.

Van Schmus, W.R., 1995. Natural radioactivity of the crust and mantle. In: Ahrens, T.J. (Ed.), A Handbook of Physical Constants: Global Earth Physics. In: AGU Reference Shelf Series, vol. 1. ISBN 0-87590-851-9. 380 pp.

Vangelov, V.I., Jarvis, G.T., 1994. Geometrical effects of curvature in axisymmetric spherical models of mantle convection. J. Geophys. Res. 99, 9345–9358.

Yoder, C.F., 1995. Astrometric and geodetic properties of Earth and the Solar System. In: Ahrens, T.J. (Ed.), A Handbook of Physical Constants: Global Earth Physics. In: AGU Reference Shelf Series, vol. 1. ISBN 0-87590-851-9, pp. 1–31.

Ward, W.R., 1981. Orbital inclination of Iapetus and the rotation of the Laplacian plane. Icarus 46, 97–107.

Wasserburg, G.J., Papanastassiou, D.A., 1982. Some short-lived nuclides in the early Solar System. In: Barnes, C.A., Clayton, D.D., Schramm, D.N. (Eds.), Essays in Nuclear Astrophysics. Cambridge Univ. Press, New York, p. 77.

Wasson, J.T., Kalleymen, G.W., 1988. Composition of chondrites. Philos. Trans. R. Soc. London A 325, 535–544.

Zaranek, S.E., Parmentier, E.M., 2004. The onset of convection in fluids with strongly temperature-dependent viscosity cooled from above with implications for planetary lithospheres. Earth Planet. Sci. Lett. 224, 371–386.

Zschau, J., 1978. Tidal friction in the solid Earth: Loading tides versus body Tides. In: Brosche, P., Sundermann, J. (Eds.), Tidal Friction and the Earth's Rotation. Springer-Verlag, Berlin, pp. 62–94.

Zuber, M.T., Smith, D.E., 1997. Mars without Tharsis. J. Geophys. Res. 102, 28673–28686.